https://doi.org/10.5194/egusphere-2023-566
Preprint. Discussion started: 28 March 2023

Predicting photooxidant concentrations in aerosol liquid water based on laboratory extracts of ambient particles

Lan Ma[1a], Reed Worland[1b], Wenqing Jiang[2], Christopher Niedek[2], Chrystal Guzman[1c], Keith J. Bein[3], Qi Zhang[2], Cort Anastasio[1]

[1]Department of Land, Air and Water Resources, University of California, Davis, One Shields Avenue, Davis, CA 95616-8627, USA
[2]Department of Environmental Toxicology, University of California, Davis, One Shields Avenue, Davis, CA 95616-8627, USA
[3]Center for Health and the Environment, University of California, Davis, One Shields Avenue, Davis, CA 95616-8627, USA
[a]Now at: SGS-CSTC Standards Technical Services Co.,Ltd. Hangzhou Branch, Hangzhou, Zhejiang Province, 310052, China
[b]Now at: Department of Chemistry, University of Washington, 1410 Northeast Campus Parkway, Seattle, WA 98195, USA
[c]Now at Department of Pharmacology, University of Washington, 1410 Northeast Campus Parkway, Seattle, WA 98195, USA

Correspondence to: Cort Anastasio (canastasio@ucdavis.edu)

Abstract. Aerosol liquid water (ALW) is a unique reaction medium, but its chemistry is poorly understood. For example, little is known of photooxidant concentrations - including hydroxyl radical ($^{\bullet}$OH), singlet molecular oxygen ($^1O_2$*), and oxidizing triplet excited states of organic matter (^{3}C*) – even though they likely drive much of ALW chemistry. Due to the very limited water content of particles, it is difficult to quantify oxidant concentrations in ALW directly. To predict these values, we measured photooxidant concentrations in illuminated aqueous particle extracts as a function of dilution and used the resulting oxidant kinetics to extrapolate to ALW conditions. We prepared dilution series from two sets of particles collected in Davis, California: one from winter (WIN) and one from summer (SUM). Both periods are influenced by biomass burning, with dissolved organic carbon (DOC) in the extracts ranging from 10 to 495 mg C L^{-1}. In the winter sample, the $^{\bullet}$OH concentration is independent of particle mass concentration, with an average value of 5.0 (± 2.2) × 10^{-15} M, while in summer $^{\bullet}$OH increases with DOC in the range (0.4 - 7.7) × 10^{-15} M. In both winter and summer samples, ^{3}C* concentrations increase rapidly with particle mass concentrations in the extracts, and then plateau under more concentrated conditions, with a range of (0.2 - 7) ×10^{-13} M. WIN and SUM have the same range of $^1O_2$* concentrations, (0.2 -

https://doi.org/10.5194/egusphere-2023-566
Preprint. Discussion started: 28 March 2023

8.5) $\times 10^{-12}$ M, but in WIN the $^1O_2$* concentration increases linearly with DOC, while in SUM $^1O_2$* approaches a plateau.

We next extrapolated the relationships of oxidant formation rates and sinks as a function of particle mass concentration from our dilute extracts to the much more concentrated condition of aerosol liquid water. Predicted •OH concentrations in ALW (including mass transport of •OH from the gas phase) are (5 - 8) $\times 10^{-15}$ M, similar to those in fog/cloud waters. In contrast, predicted concentrations of ^3C* and $^1O_2$* in ALW are approximately 10 to 100 times higher than in cloud/fogs, with values of (4 – 9) $\times 10^{-13}$ M and (1 – 5) $\times 10^{-12}$ M, respectively. Although •OH is often considered the main sink for organic compounds in the atmospheric aqueous phase, the much higher concentrations of ^3C* and $^1O_2$* in aerosol liquid water suggest these photooxidants will be more important sinks for many organics in particle water.

1. Introduction

The chemical processing of organic compounds in cloud/fog water and aerosol liquid water is an important source and sink of secondary organic aerosol (SOA) (Ervens et al., 2011; Gilardoni et al., 2016; Lim et al., 2010; McNeill, 2015). Aerosol liquid water (ALW), i.e., the liquid-phase water on airborne particles, is much less abundant (in terms of liquid water content) and contains much higher concentrations of solutes, compared to clouds and fogs. ALW appears to be an efficient and important medium for the production of aqueous SOA (aqSOA) (Ervens and Volkamer, 2010; Faust et al., 2017; Volkamer et al., 2007; Wu et al., 2018; Zhang et al., 2011) and ALW chemistry is often different from that in more dilute cloud and fog drops (Ervens, 2018; Mekic et al., 2018; Zhou et al., 2019). For example, reactions in ALW can more efficiently produce high molecular-weight compounds like oligomers and brown carbon (De Haan et al., 2020; Lim et al., 2010; Renard et al., 2014; Tan et al., 2012; Xia et al., 2018). Modeled rates of aqSOA formation in ALW vary enormously, likely because reactant concentrations and chemical processes in particle water are poorly understood (Ervens and Volkamer, 2010; Ervens, 2018; Lin et al., 2014; Washenfelder et al., 2011).

A key driver of ALW reactivity is likely the concentrations of photochemically-generated oxidants (Herrmann et al., 2015; Lim et al., 2010). Important aqueous photooxidants include hydroxyl radical (•OH), oxidizing triplet excited states of organic compounds (^3C*), and singlet molecular oxygen ($^1O_2$*) (Kaur et al., 2019). •OH is the most widely studied oxidant due to its ubiquity and high reactivity: it reacts with most organics with near diffusion-controlled rate constants (Herrmann et al., 2015). The main sources of aqueous •OH include mass

https://doi.org/10.5194/egusphere-2023-566
Preprint. Discussion started: 28 March 2023

transfer from the gas phase, the photo-Fenton reaction, and photolysis of nitrate, nitrite, and other species (Anastasio and McGregor, 2001; Arakaki and Faust, 1998; Badali et al., 2015; Herrmann et al., 2010; Tilgner and Herrmann, 2018), while the main sinks of •OH are dissolved organic compounds (Anastasio and Newberg, 2007; Arakaki et al., 2013). Based on lab studies of clouds, fogs, and aqueous particle extracts, concentrations of •OH in atmospheric waters (including calculated rates of gas-to-particle partitioning of •OH) are typically 10^{-16} – 10^{-15} M (Anastasio and McGregor, 2001; Anastasio and Newberg, 2007; Arakaki et al., 2013; Faust and Allen, 1993; Kaur et al., 2019; Zhou et al., 2008). In contrast, modeled •OH concentrations in aqueous aerosol are generally 10^{-13} to 10^{-12} M (Ervens et al., 2014; Tilgner and Herrmann, 2018; Tilgner et al., 2013), but these are likely overestimates, in part because of missing •OH sinks (Arakaki et al., 2013; Arciva et al., 2022).

When organic chromophores (i.e., brown carbon) absorb sunlight, the molecules are promoted to their more reactive, triplet excited states, some of which are oxidants (Kaur et al., 2019; McNeill and Canonica, 2016). These oxidizing triplets can transform numerous atmospheric species, including converting phenols and biogenic volatile compounds to aqSOA, and oxidizing sulfite to sulfate (González Palacios et al., 2016; Monge et al., 2012; Rossignol et al., 2014; Smith et al., 2014; Wang et al., 2020). ^{3}C* can be important oxidants in atmospheric and surface waters, with concentrations of 10^{-15}-10^{-13} M (Kaur and Anastasio, 2018; Kaur et al., 2019; McNeill and Canonica, 2016). In comparison, triplet concentrations in ALW are expected to be higher because the production rate of ^{3}C* increases with dissolved organic carbon (Canonica and Freiburghaus, 2001; McCabe and Arnold, 2017), although organic compounds can also be important sinks for ^{3}C*, suppressing its steady-state concentration (Gemayel et al., 2021; Wenk et al., 2013). This dual effect of organic compounds makes it difficult to predict ^{3}C* concentrations in ALW. Kaur et al. (2019) estimated a concentration of oxidizing ^{3}C* in ALW of 10^{-13} to 10^{-11} M based on measurements in dilute particle extracts, while Tilgner et al. (2021) estimated the ALW concentration of triplets as 10^{-11} M.

Most or all of atmospheric triplets (i.e., both oxidizing and non-oxidizing triplets) also transfer energy to dissolved oxygen to form another important photooxidant, singlet molecular oxygen. $^1O_2$* concentrations in fog/cloud drops and dilute extracts of ambient particles and lab SOA are higher than •OH and ^{3}C*, typically 10^{-14} to 10^{-12} M (Anastasio and McGregor, 2001; Bogler et al., 2022; Faust and Allen, 1992; Kaur and Anastasio, 2017; Kaur et al., 2019; Li et al., 2019; Manfrin et al., 2019). Though $^1O_2$* is generally less reactive than •OH and ^{3}C*, it can react quickly with electron-rich compounds and can be a competitive oxidant because of its high concentration.

https://doi.org/10.5194/egusphere-2023-566
Preprint. Discussion started: 28 March 2023

Kaur et al. (2019) estimated $^1O_2$* might be as high as 10^{-10} M under ALW conditions due to increased ^{3}C* concentrations, which would make it an important oxidant in particle water (Ma et al., 2021).

Due to its limited water content, it is difficult to study chemistry in ALW directly. To get around this problem, Kaur et al. (2019) measured •OH, ^{3}C*, and $^1O_2$* kinetics as a function of dilution in extracts of a single PM sample and extrapolated the results to aqueous aerosol conditions. However, there are large uncertainties with this extrapolation since the PM extracts were approximately 1000 times more dilute than ALW conditions. In addition, these authors only examined a single sample collected during winter and did not correct their triplet results for probe inhibition by organic compounds. To revisit this approach and, we hope, reduce uncertainty, here we apply the same method but with higher dissolved organic matter concentrations in particle extracts and with correction for triplet probe inhibition. Moreover, in this work we study both a winter PM sample as well as summer wildfire particles to explore differences in oxidant kinetics.

2. Experimental methods

2.1 Chemicals

Furfuryl alcohol (FFA, 98%), benzoic acid (BA, ≥ 99.5%), *p*-hydroxybenzoic acid (*p*-HBA, 99%) (phenylthiol)acetic acid (PTA, 96%), syringol (SYR, 99%), 3,4-dimethoxybenzaldehyde (DMB, 99%), and deuterium oxide (99.9% D-atom) were received from Millipore Sigma. All chemical solutions and particulate matter extracts were prepared using air-saturated ultrapure water (Milli-Q water) from a Milli-Q Advantage A10 system (Millipore; ≥ 18.2 MΩ cm) with an upstream cartridge to remove organics.

2.2 Particle collection and extraction

Fine particles ($PM_{2.5}$) were collected on the roof of Ghausi Hall on the campus of the University of California, Davis in February and August 2020. Davis air quality in winter is often impacted by residential wood combustion, while the August 2020 samples were impacted by Northern California wildfires. $PM_{2.5}$ was collected using a high-volume sampler equipped with a PM_{10} inlet (Graseby Andersen) and two offset, slotted impactor plates (Tisch Environmental, Inc., 230 series) to remove coarse particles. The resulting fine particles were collected onto Teflon-coated borosilicate glass microfiber filters (Pall Corporation, EmFab™ filters, 8 in. × 10 in.) that were pre-cleaned by gently shaking in Milli-Q water for 8 h and then drying at 100 °C. During sampling, the airflow rate was maintained at 68 (±2) m^3 per hour. Particles were either collected for 24 h or up to a week; see Table S1 for

https://doi.org/10.5194/egusphere-2023-566
Preprint. Discussion started: 28 March 2023

details. Upon collection, each sample was wrapped in aluminum foil (baked previously at 500 °C for 8 h), sealed in a Ziploc bag, and frozen at −20 °C. Field blanks were obtained in an identical manner as samples, including loading the clean filters into the sampler and turning on the pump for 2 min.

To prepare particulate matter extracts (PMEs), filters were cut into 2 cm × 2 cm squares on the day of extraction. Each square was placed in an individual, sealed, 20-mL amber glass vial and extracted with Milli-Q water by shaking for 4 h in the dark. The extracts from the same filter sample were combined, filtered (0.22 μm PTFE; Pall), and adjusted to pH 4.2 with sulfuric acid or sodium hydroxide to mimic the acidity of winter particle water in the Central Valley of California (Parworth et al., 2017). The pH of each extract was measured by a pH microelectrode (MI-414 series, protected tip; Microelectrodes, Inc.). The UV-Vis spectrum of each PME was measured in a 1-cm cuvette immediately after pH adjustment with a Shimadzu UV-2501PC spectrophotometer. Rates of sunlight absorption between 300 and 450 nm were calculated for midday winter-solstice sunlight in Davis, as described by Kaur et al. (2019). PMEs were divided into 4-mL HDPE bottles and flash-frozen in liquid nitrogen immediately after preparation and were later thawed on the day of experiments. Filter squares were weighed by a microbalance (Sartorius M2P) before and after extraction to determine the PM mass extracted; the resulting PM mass/water mass ratios in the filtered extracts might be overestimated because of removal of insoluble material during filtration. Dissolved organic carbon (DOC) and major ion concentrations (Table S2) in PMEs were measured by a Shimadzu TOC-VCPH analyzer and Metrohm ion chromatographs (881 Compact IC Pro) equipped with conductivity detectors, respectively.

To investigate the relationship between particle dilution and oxidant concentration, filter squares from the same sample were extracted with five different volumes of Milli-Q water: 10, 2, 0.7, 0.4, and 0.3 mL. To obtain enough filter squares for this dilution series, for both the winter (WIN) and summer (SUM) samples we combined extracts from 180 filter squares cut from three sheets of filter that were collected on consecutive days. The same number of squares were cut from each of the three filters in a given sample. We use “PME name-water volume” (e.g., WIN-0.7) to denote the sample and extraction volume. Because it is difficult to extract squares with only 0.4 or 0.3 mL of Milli-Q, for these dilutions we extracted each filter square with 1 mL of Milli-Q and then used a rotary evaporator (Buchi Rotavapor R-110; temperature set no higher than 65 °C) to remove water until we obtained the equivalent of a 0.4 or 0.3 mL extract. We define the concentration factor (CF) of an extract as the inverse of the volume used for extraction. For example, WIN-10 has a concentration factor of 0.1.

https://doi.org/10.5194/egusphere-2023-566
Preprint. Discussion started: 28 March 2023

2.3 Sample illumination and chemical analysis

We illuminated samples with light from a 1000 W xenon arc lamp passed through a water filter, an AM1.0 air mass filter (AM1D-3L, Sciencetech), and a 295 nm long-pass filter (20CGA-295, Thorlabs) to simulate tropospheric sunlight (Kaur and Anastasio, 2017). We first transferred the extract into a silicone-plugged GE 021 quartz tube (5 mm inner diameter, 1.0 mL volume) and then spiked it with the photooxidant probe and mixed it. The entire tube was illuminated at 20 °C and was not stirred. Dark control samples were wrapped in aluminum foil and kept in the same photoreactor chamber. During illumination, approximately 150 µL aliquots were removed from the illuminated and dark tubes at specific time intervals to measure concentrations of probes with high-performance liquid chromatography (HPLC, Shimadzu LC-20AB pump, Thermo Scientific Accucore XL C18 column (50 × 3 mm, 4 µm bead), and Shimadzu-M20A UV-Vis detector). The photon flux on each experiment day was determined by measuring the photolysis rate constant of a 10 µM 2-nitrobenzaldehyde (2NB) solution in the same type of container as samples (Galbavy et al., 2010).

2.4 Photooxidant measurements

Details about determining photooxidant concentrations are provided in past papers (Anastasio and McGregor, 2001; Kaur and Anastasio, 2017; Kaur et al., 2019) and are only discussed briefly here.

2.4.1 Hydroxyl radical (•OH)

The production rate, rate constant for loss, and steady-state concentration of •OH were quantified using benzoic acid (BA) and a competition kinetics technique. A 0.020 M stock solution of benzoic acid/benzoate was prepared and adjusted to pH 4.2. For each sample, four 1.0-mL aliquots of PME were spiked with different final concentrations (100 – 1200 µM) of BA, keeping PME dilution by the addition of probe to less than 10%. We then illuminated each PME and used HPLC to monitor the formation of *p*-hydroxybenzoic acid (*p*-HBA), which is formed from BA oxidation by •OH. The initial rate of *p*-HBA formation was determined from a regression between concentration and illumination time, using either a linear regression or, for plots with curvature, a three-parameter exponential fit

$$[p\text{-}HBA]_t = [p\text{-}HBA]_0 + a(1 - e^{-bt}) \quad (1)$$

https://doi.org/10.5194/egusphere-2023-566
Preprint. Discussion started: 28 March 2023

where [*p*-HBA]$_t$ and [*p*-HBA]$_0$ are the concentrations at illumination times *t* and zero, respectively, and *a* and *b* are regression fit parameters. For exponential kinetics data, the initial formation rate of *p*-HBA, $R_{P,EXP}$, was calculated with

$$R_{P,EXP} = a \times b \quad (2)$$

Rates of *p*-HBA formation were normalized to sunlight conditions at midday on the winter solstice at Davis (solar zenith angle = 62°; $j_{2NB,win}$ = 0.0070 s^{-1} (Anastasio and McGregor, 2001)), and corrected for internal light screening due to sample absorption, using

$$R_{P,norm} = \left[\frac{R_{P,EXP}}{S_\lambda \times j_{2NB,EXP}}\right] \times j_{2NB,win} \quad (3)$$

where S_λ is the internal light screening factor in an individual sample (Table S1) and $j_{2NB,exp}$ is the photolysis rate constant of 2NB measured on the experiment day.

We then fitted $1/R_{P,norm}$ versus 1/[BA] with a linear regression and used the slope and *y*-intercept to calculate the initial production rate of •OH (P_{OH}), the pseudo first-order rate constant of •OH loss by natural sinks (k'_{OH}), and the steady-state •OH concentration

$$P_{OH} = \frac{1}{y - intercept \times Y_{pHBA}} \quad (4)$$

$$k'_{OH} = k_{BA+\cdot OH}\left(\frac{slope}{y - intercept}\right) \quad (5)$$

$$[^{\bullet}OH] = \frac{1}{k_{BA+\cdot OH} \times slope \times Y_{p\text{-}HBA}} \quad (6)$$

Here $Y_{p\text{-HBA}}$ (0.18) is the yield of *p*-HBA from the reaction of BA with •OH (Anastasio and McGregor, 2001) and $k_{BA+\cdot OH}$ is the second-order rate constant of BA reacting with •OH at pH 4.2 (5.1 × 10^9 M^{-1} s^{-1}) (Ashton et al., 1995; Wander et al., 1968). •OH measurements are in Table S3.

https://doi.org/10.5194/egusphere-2023-566
Preprint. Discussion started: 28 March 2023

2.4.2 Oxidizing triplet excited states of organic matter ($^3C^*$)

Triplets were measured employing syringol (SYR) and (phenylthio)acetic acid (PTA) as probes (Kaur and Anastasio, 2018; Ma et al., 2023). SYR captures both weakly and strongly oxidizing triplets, but its decay can be inhibited by dissolved organic matter (DOM) in PME (Canonica and Laubscher, 2008; Ma et al., 2023; Wenk and Canonica, 2012; Wenk et al., 2015). In contrast, PTA is less sensitive to inhibition by DOM, but it only reacts appreciably with strongly oxidizing triplets (Ma et al., 2023). Two 1.0 mL aliquots of PME were spiked with 10 µM of SYR or PTA, and then illuminated to determine the pseudo-first order rate constants for loss of each probe ($k'_{P,EXP}$). Next, $k'_{P,EXP}$ values were normalized to Davis winter sunlight conditions and corrected for light screening using an equation analogous to Eq. 3 to obtain rate constant k'_P. The contributions of direct photodegradation, $^\bullet OH$, and $^1O_2$* to probe decay were then subtracted to determine the rate constant for loss of probe due to triplets, $k'_{P,3C*}$

$$k'_{P,^3C^*} = k'_P - \left(j_P + k_{P+OH}[^\bullet OH] + k_{P+1O2*}[^1O_2{}^*]\right) \quad (7)$$

Here j_P is the probe direct photodegradation rate constant under Davis winter sunlight, and k_{P+OH} and k_{P+1O2*} are the bimolecular rate constants of probe reacting with $^\bullet OH$ and $^1O_2$*, respectively (Table S4). $^\bullet OH$ accounts for 2% - 35% and 3% - 17% of the decay of SYR and PTA, respectively, while $^1O_2$* accounts for 3% - 45% and 2% - 10% for SYR and PTA (Tables S5 and S6). Since triplets in PMEs represent the excited states of a complex mixture of brown carbon, there is no single value for the second-order rate constant of ^3C* reacting with probes (k_{P+3C*}). To estimate triplet concentrations, we assume that ^3C* in PME have the same average reactivity as the triplet state of 3,4-dimethoxybenzaldehyde, ^{3}DMB* (Fleming et al., 2020; Kaur and Anastasio, 2018; Kaur et al., 2019). Unlike our past work (Kaur et al., 2019), we corrected for DOM inhibiting the decays of SYR and PTA, which can cause an underestimate of ^3C* concentrations. To do this, we measured the inhibition factor (*IF*) in samples (Canonica and Laubscher, 2008; Ma et al., 2023; Wenk et al., 2011) and used it to correct the ^3C* concentration. Details about inhibition factor measurements and [^3C*] corrections are in Supplemental Section S1. The ^3C* concentration after inhibition correction is

$$[^3C^*]_P = \frac{k'_{P,3C*}}{k_{P+3DMB*} \times IF_{P,corr}} \quad (8)$$

where $k_{P+3DMB*}$ is the second-order rate constant of probe with ^{3}DMB* (Table S4), and $IF_{P,corr}$ is the inhibition factor of the probe in that extract (Table S7). ^3C* concentrations in the main text are values after *IF* correction.

https://doi.org/10.5194/egusphere-2023-566
Preprint. Discussion started: 28 March 2023

While our past work indicates that ^{3}DMB* is a good surrogate for the average oxidizing triplet in Davis drops and particles (Kaur and Anastasio, 2018; Kaur et al., 2019), it is possible that $k_{P+3DMB*}$ is higher than the rate constant for probe with natural triplets. This is the case for surface waters, where the 2,4,6-trimethylphenol (TMP) + ^{3}DMB* rate constant (Ma et al., 2023) is three times higher than the TMP + ^{3}CDOM* rate constant (Erickson et al., 2018). If this is also the case for our PM extracts, we would be underestimating oxidizing triplet concentrations by roughly a factor of three.

2.4.3 Singlet molecular oxygen ($^1O_2$*)

We used FFA as a probe to determine $^1O_2$* concentrations (Anastasio and McGregor, 2001; Haag et al., 1984). 1.0 mL of PME sample was divided into two 0.5 mL aliquots, and then one was diluted with 0.5 mL H_2O while the other was diluted with 0.5 mL deuterium oxide (D_2O). 10 µM FFA was spiked into each solution and then both were illuminated. The pseudo-first-order rate constant of FFA loss in H_2O- and D_2O-diluted PME ($k'_{FFA,H2O}$ and $k'_{FFA,D2O}$) during illumination was determined as the negative slope of a linear regression between $\ln([FFA]_t/[FFA]_0)$ versus illumination time (t). The $^1O_2$* concentration in the undiluted PME was determined from the difference of FFA loss rates in H_2O and D_2O using (Anastasio and McGregor, 2001)

$$[^1O_2{}^*]_{EXP} = \frac{k'_{FFA,D2O} - k'_{FFA,H2O}}{D \times k_{FFA+1O2*} \times \left(\frac{k'_{H2O}}{k'_{H2O}\chi_{H2O} + k'_{D2O}\chi_{D2O}} - 1\right)} \quad (9)$$

where D is the sample dilution factor (i.e., 0.5 for our experiments); $k_{FFA+1O2*}$ is the second-order rate constant of FFA reacting with $^1O_2$* at 20 °C, 0.96 (± 0.04)×10^8 M^{-1} s^{-1} (Appiani et al., 2017); k'_{H2O} and k'_{D2O} are the first-order rate constants for loss of $^1O_2$* in 100% H_2O (2.2 × 10^5 s^{-1}) and D_2O (1.6 × 10^4 s^{-1}), respectively (Bilski et al., 1997); and χ_{H2O} and χ_{D2O} are the mole fractions of H_2O and D_2O in the D_2O-diluted solution. Analogous to equation 3, we normalized the experimentally determined $^1O_2$* concentrations using the light screening factor of each PME and to Davis winter sunlight conditions. $^1O_2$* measurements are in Table S8.

3. Results and discussions

3.1 Testing extraction and rotary evaporation

Our winter particle filters were collected in February 2020, when Davis was influenced by residential wood combustion; the average $PM_{2.5}$ concentration during our sampling was 9.2 µg m^{-3}. The summer particles were

https://doi.org/10.5194/egusphere-2023-566
Preprint. Discussion started: 28 March 2023

collected in August 2020, when severe wildfires were occurring approximately 30 km from Davis, resulting in an average $PM_{2.5}$ concentration of 54 μg m^{-3}. Figure 1 shows the dissolved organic carbon (DOC) concentrations and rates of light absorption (R_{abs}) as a function of dilution in the winter (WIN) and summer (SUM) particle extracts. We express dilution as the ratio of dry particle mass to liquid water mass in our extracts since we can experimentally measure these quantities for our PMEs and can estimate values for both clouds/fogs and airborne particles. Both DOC and R_{abs} are directly proportional to particle mass/water mass ratio, indicating that the extractions of filter squares with varying volumes of water achieved the same extraction efficiency. The DOC values of the most concentrated extracts (-0.4 and -0.3) also follow the linear relationship, showing that the rotary evaporation process used for these dilutions did not lead to significant loss of brown carbon or other organic compounds. As shown in Figure S1, UV-Vis spectra of the -0.4 and -0.3 extracts before and after rotovapping are essentially the same, indicating that evaporation did not change the BrC composition significantly.

We also examined if rotovapping affects photooxidant concentrations. First, we extracted one filter either with 0.7 mL water/square (sample PME-NR) or 2 mL water/square followed by rotovapping to the equivalent of 0.7 mL/square (sample PME-R). In a second test, we diluted a rotovapped sample (WIN-0.3) by a factor of 6.7 with water to obtain an extract equivalent to 2 mL Milli-Q/square (WIN-0.3D); this diluted, rotovapped sample should be equivalent to WIN-2, a not-rotovapped sample with the same overall dilution. Figure S2 presents photooxidant concentrations in the two tests. In each test, the concentrations are essentially the same in the rotovapped and not rotovapped samples, indicating a negligible effect of rotary evaporation on photooxidant kinetics.

https://doi.org/10.5194/egusphere-2023-566
Preprint. Discussion started: 28 March 2023

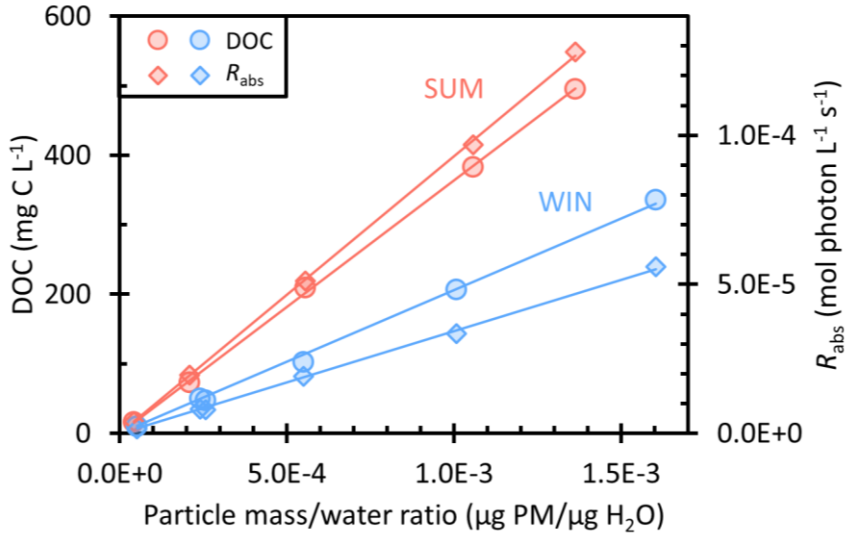

Figure 1. Dependence of dissolved organic carbon (DOC, circles) and rate of sunlight absorption between 300 – 450 nm (R_{abs}, diamonds) on particle mass/water mass ratio (i.e., aqueous particle concentration) in summer (red) and winter (blue) particle extracts.

3.2 Ions and light absorption

Figure 1 shows that summer and winter PMEs have DOC concentrations in the range of 16 – 495 and 10 – 336 mg C L^{-1}, respectively, but WIN has slightly higher particle mass/water ratios, (0.05 – 1.6) × 10^{-3} µg PM/µg H_2O, compared to (0.04 – 1.4) × 10^{-3} µg PM/µg H_2O for SUM. The summer wildfire sample shows a higher average fraction of organic carbon to PM mass, 0.37 (± 0.02), compared to winter (0.20 ± 0.01). The OC/PM ratio in SUM, which represents relatively fresh aerosols from wildfires, is lower than the typical values near 0.5 for biomass burning particles (Reid et al., 2005; Schauer et al., 2001), probably because our water extractions did not fully solubilize non-polar organic compounds from the particles. The winter sample has lower organic carbon but higher concentrations of ions, including nitrate (NO_3^-), sulfate (SO_4^{2-}), and ammonium (NH_4^+) (Table S2). For example, nitrate concentrations in WIN range from 0.18 to 5.2 mM and contribute on average (± 1 σ) 20 (± 2) % of the total extracted PM mass. In contrast, NO_3^- concentrations in SUM are about five times lower (0.03 – 1.0 mM) at the same concentration factor and only contribute an average of 4.4 (± 0.4) % of the SUM PM mass. The sulfate in WIN accounts for 11 (± 4) % of extracted PM mass, with concentrations (0.03 – 2.3 mM) around 4 times higher than in SUM (0.02 – 0.6 mM, accounting for an average of 4.2 (± 0.6) % of extracted PM mass). NH_4^+ is also higher in WIN (0.20 – 3.6 mM) compared to SUM (0.10 – 1.3 mM). Sodium concentrations in both WIN and

https://doi.org/10.5194/egusphere-2023-566
Preprint. Discussion started: 28 March 2023

SUM are high and comparable to ammonium, with ranges of 0.2 – 3.6 mM and 0.1 – 1.7 mM, respectively. Concentrations of potassium, a tracer of biomass burning (Andreae, 1983), are 0.03 – 0.7 mM in both WIN and SUM, with a K/PM mass ratio of 0.02 (±0.004), in the range reported for biomass burning aerosols, 0.02 to 0.05 (Reid et al., 2005; Urban et al., 2012).

For all PMEs, absorbance declines exponentially with wavelength (e.g., Fig. S1), and WIN and SUM samples have the same average absorption Ångström exponent (AAE, 300 – 450 nm) of 7.2 (Table S1), comparable to AEE values (6 – 8) previously reported in water extracts of biomass burning particles (Hecobian et al., 2010; Hoffer et al., 2006; Kaur et al., 2019). The pathlength-normalized absorption coefficient at 300 nm (α_{300}) for the summer samples (0.2 – 6.7 cm^{-1}) is about 2 times higher than winter samples at the same concentration factor (0.1 – 3.0 cm^{-1}) (Table S1). Thus, summer extracts absorb sunlight at approximately twice the rate as winter extracts (Figure 1). We also calculated the dissolved organic carbon-normalized mass absorption coefficient (MAC_{DOC}) of each extract by dividing the absorbance at 300 or 365 nm by the DOC concentration (Kaur et al., 2019). SUM average MAC_{DOC} values across all dilutions are 3.1 (± 0.1) and 1.0 (± 0.1) m^2 (g C)$^{-1}$ at 300 and 365 nm, respectively, which are approximately 1.5 times higher than the WIN values (Table S1). This difference is likely because the SUM sample is dominated by fresh wildfire organic aerosols that are composed of organic compounds with a higher degree of unsaturation, increasing light absorption (Fleming et al., 2020). Meanwhile, the WIN sample may contain a lower fraction of fresh biomass burning aerosols due to oxidation and photobleaching of the brown carbon (Forrister et al., 2015; Wong et al., 2019). Our MAC value for WIN is similar to the average MAC value in the previous Davis winter samples (Kaur et al., 2019).

3.3 Photooxidants in PM extracts

In this section we first present our measured oxidant concentrations as a function of particle dilution in the WIN and SUM extracts. We use DOC as the independent variable in our plots because BrC likely dominates the production of $^3C^*$ and $^1O_2^*$ and DOC is proportional to concentration factor in each extract series. We then examine how the production rate (P_{OX}) and rate constant for loss (k'_{OX}) for each oxidant vary as a function of dilution. These parameters are related to the oxidant steady-state concentration, [OX], by

$$[OX] = \frac{P_{ox}}{k'_{ox}} \quad (10)$$

https://doi.org/10.5194/egusphere-2023-566
Preprint. Discussion started: 28 March 2023

In the next section (3.4), we extrapolate these kinetic parameters to aerosol liquid water conditions to predict photooxidant concentrations in ALW.

3.3.1 Hydroxyl radical in PM extracts

As shown in Fig. 2a, the most dilute sample in the WIN dilution series, WIN-10, has the lowest •OH concentration, while in the other dilutions [•OH] is noisy but appears independent of DOC. This result, that •OH concentration is essentially independent of particle mass concentration, is similar to what Kaur et al. (2019) observed for winter samples (green points in Fig. 2), although our •OH concentrations are approximately 10 times higher.

Kaur et al. (2019) found that the •OH photoproduction rate (P_{OH}) and sink ($\underline{k'}_{OH}$) both linearly increase with concentration factor, leading to a roughly constant •OH concentration since the concentration is equal to the ratio P_{OH}/k'_{OH} (Eq. 10). To explore this in our samples, we determined P_{OH} and k'_{OH} in all of the WIN and SUM extracts; we start by considering the WIN results. As shown in Fig. 3a, P_{OH} and k'_{OH} both increase linearly with DOC, consistent with the winter PM extract observations of Kaur et al. (2019), though our samples have a higher slope for P_{OH} but a lower one for k'_{OH}. This higher •OH production rate, coupled with a lower rate constant for •OH loss, is responsible for the roughly 10 times higher [•OH] in this work, but we do not know why these parameters are so different between the previous and current winter particle samples. P_{OH} in WIN ranges from 0.02 $\times 10^{-8}$ to 4.8 $\times 10^{-8}$ M s^{-1}, significantly higher than typical values (approximately 10^{-10} M s^{-1}) in cloud and fog waters (Arakaki et al., 2013; Kaur and Anastasio, 2018; Tilgner and Herrmann, 2018). In Davis fog samples, the major source of •OH is photolysis of nitrate and nitrite (Anastasio and McGregor, 2001; Kaur and Anastasio, 2017). However, in our winter PM extracts, nitrate accounts for 10% or less of P_{OH} (Table S3), while the nitrite contribution is negligible. Instead, we hypothesize that our samples might contain higher concentration of transition metals, contributing to •OH production (Vidrio et al., 2009). While DOC photoreactions also can be a source of •OH (Badali et al., 2015), it seems likely that P_{OH} is correlated with DOC primarily because DOC is a proxy for concentration factor in the extracts. As for •OH sinks in our WIN extracts, k'_{OH} is in the range (0.2 – 9.9) $\times 10^{6}$ s^{-1}, higher than previous Davis fog values ((0.4 – 1.3) $\times 10^{6}$ s^{-1}; (Kaur and Anastasio, 2017)). The lowest k'_{OH} (in WIN-10, the most dilute extract) is comparable to the field blank values (Table S3), suggesting that [•OH] in WIN-10 may be artificially low because of background contamination. We also calculated the rate constant of organics reacting with •OH (k_{DOC+OH}) for the winter samples; our average WIN value, 2.4 (± 0.7) × 10^{8} L (mol C)$^{-1}$ s^{-1}, is similar to the one determined by Arakaki et al. (2013) for general atmospheric waters, 3.8 (± 1.9) × 10^{8} L

https://doi.org/10.5194/egusphere-2023-566
Preprint. Discussion started: 28 March 2023

(mol C)$^{-1}$ s^{-1}. In contrast, the average winter k_{DOC+OH} in Kaur et al. (2019) is approximately three times higher than our current winter sample; i.e., the past organics were more reactive with •OH.

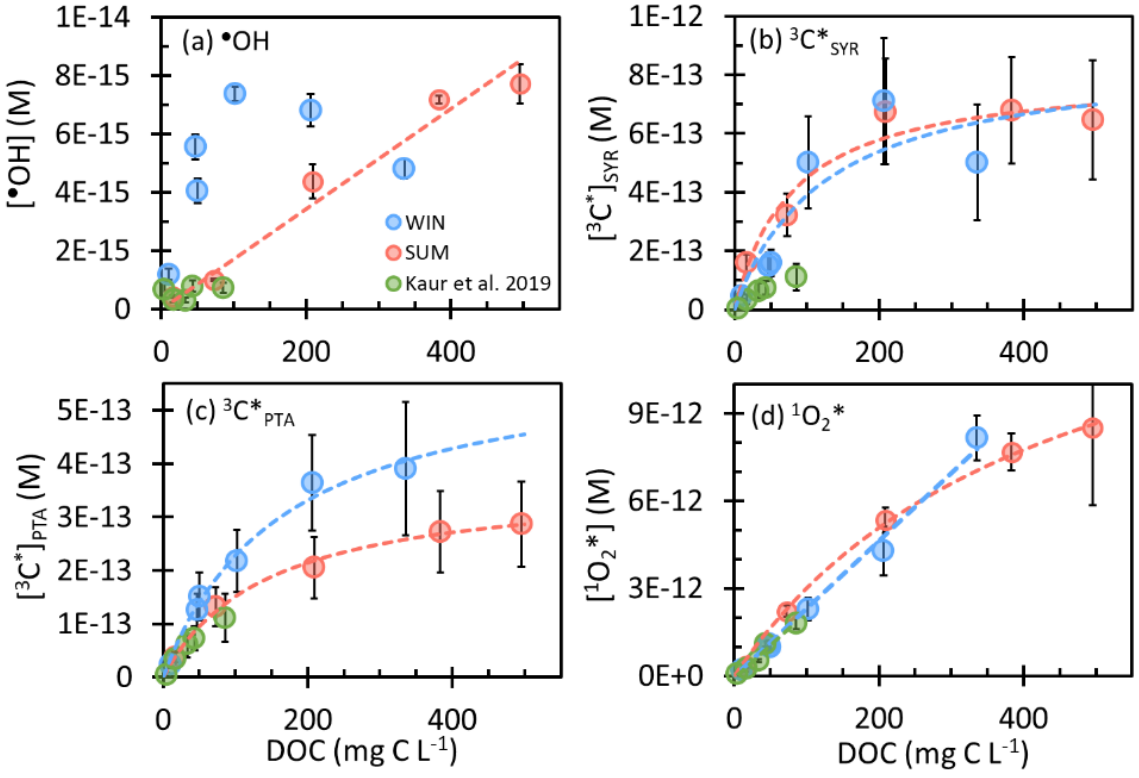

Figure 2. Steady-state concentrations of (a) hydroxyl radical, oxidizing triplet excited states of brown carbon determined by (b) SYR and (c) PTA, and (d) singlet molecular oxygen in WIN (blue) and SUM (red) samples as a function of dissolved organic carbon. WIN-0.3D results are also included. Previous measurements in Davis winter particle extracts are shown in green (Kaur et al., 2019). Error bars represent ± 1 standard error propagated from linear regression and uncertainties in rate constants. Dashed lines represent linear or hyperbolic regression fits for WIN and SUM samples.

https://doi.org/10.5194/egusphere-2023-566
Preprint. Discussion started: 28 March 2023

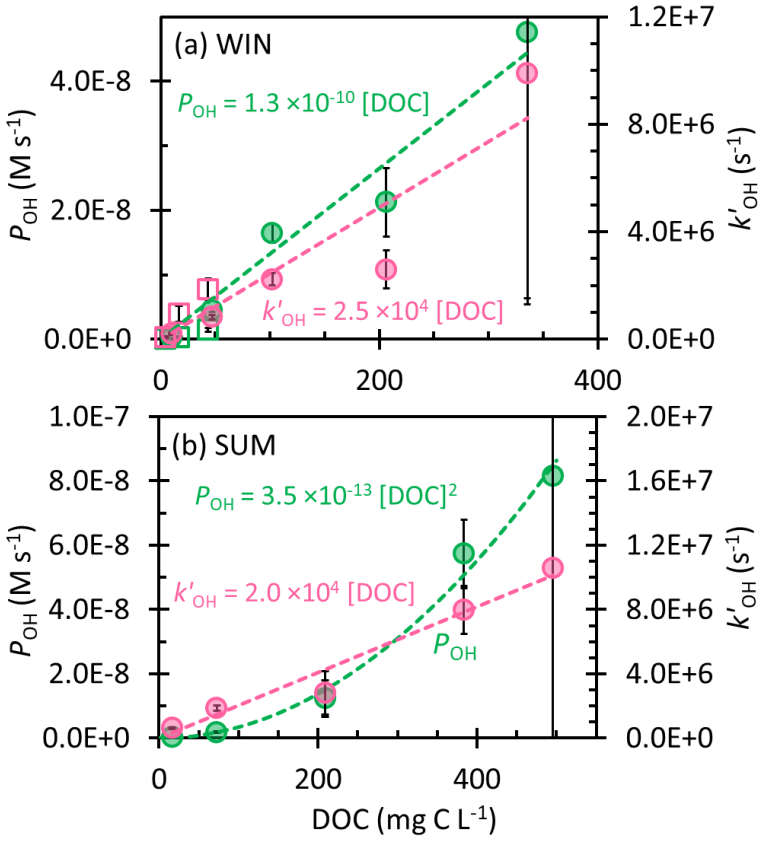

Figure 3. Dependence of rate of •OH photoproduction (P_{OH}; green, left y-axis) and rate constant for loss of •OH due to natural sinks (k'_{OH}; pink, right y-axis) on dissolved organic carbon in the (a) winter and (b) summer samples. Error bars represent ±1 standard error propagated from the error in regressions and rate constants; error bars for the 0.3 mL extracts (highest DOC) extend past the plot borders. Dashed lines represent linear regression fits, except the green dashed line in (b) SUM that is derived from the linear regression of P_{OH} with [DOC]^2. Previous measurements in Davis winter particle extracts are shown as open squares in panel (a) (Kaur et al., 2019).

Unlike WIN, •OH in the summer samples linearly increases with concentration factor or DOC, with an •OH concentration range of (0.4 – 7.7) ×10^{-15} M (Fig. 2a). This indicates that either P_{OH} or k'_{OH} does not increase linearly with DOC. As shown in Fig. 3b, k'_{OH} is linear with DOC, but P_{OH} is proportional to the DOC concentration squared. Our interpretation is that •OH production in SUM is a bimolecular reaction rather than a first-order photolysis. The most likely candidate is the photo-Fenton reaction involving soluble reduced iron and hydrogen

https://doi.org/10.5194/egusphere-2023-566
Preprint. Discussion started: 28 March 2023

peroxide (or organic peroxides) (Paulson et al., 2019; Zepp et al., 1992), where the concentrations of both reactants increase with concentration factor, as does [DOC]. Therefore, although WIN and SUM have roughly similar $^{\bullet}$OH concentrations, they apparently have different mechanisms governing $^{\bullet}$OH formation. P_{OH} in SUM is in the range (0.03 - 8.2) $\times 10^{-8}$ M s^{-1}, with the value in SUM-0.3 nearly double that of WIN-0.3. In contrast, $^{\bullet}$OH sinks for the summer and winter samples are similar (Fig. 3) and the average k_{DOC+OH} value in SUM is 2.9 (± 1.1) × 10^{8} L (mol C)$^{-1}$ s^{-1}, not significantly different from the WIN value.

3.3.2 Oxidizing triplet excited states of organic matter in PM extracts

We determined oxidizing triplet concentrations using two probes. SYR is highly reactive towards both strongly and weakly oxidizing triplets, but its decay by ^{3}C* can be inhibited by DOM, leading to an underestimate of ^{3}C* concentrations (Canonica and Laubscher, 2008; Maizel and Remucal, 2017; Wenk et al., 2011). PTA that has a higher oxidation potential (1.47 V vs. SHE, estimated using the Marcus equation) SYR (~1.17 V vs. SHE) (Canonica et al., 2000; Chellamani and Sengu, 2008), is less reactive than SYR with weakly oxidizing triplets (and thus does not capture the whole oxidizing triplet pool), but its advantage is that it is more resistant to inhibition by DOM (Klein et al., 2006; Ma et al., 2023). For both probes, we correct for probe inhibition by measuring the inhibition factor (*IF*) and using it to correct ^{3}C* concentrations (Section S1 and Table S7). Inhibition factors of SYR are as low as 0.13 (± 0.03) in the most concentrated sample (WIN-0.3), indicating that approximately 87 (± 20) % of SYR decay is inhibited by DOM in this sample, which would lead to a ^{3}C* concentration that is 7.5 (± 1.7) times lower than the actual value if there was no correction for inhibition. As for PTA, *IF* values are all greater than 0.9, indicating little inhibition. For simplicity, we only show ^{3}C* concentrations after inhibition factor correction; uncorrected values are given in Tables S5 and S6.

^{3}C* concentrations as a function of DOC are in Figure 2. With SYR as the triplet probe (Fig. 2b), the $[^{3}C^*]_{SYR}$ range is (0.5 – 7.1) $\times 10^{-13}$ M in WIN and (1.6 – 6.8) $\times 10^{-13}$ M in SUM. At the same DOC, $[^{3}C^*]_{SYR}$ values in summer and winter are similar, despite the differences in sample composition (Table S5). Oxidizing triplet concentrations in our samples are generally higher than those from Kaur et al. (2019) (Fig. 2c, green points), which can be attributed to higher DOC in our samples and our correction for SYR inhibition. From PTA, the $[^{3}C^*]_{PTA}$ range is (0.2 – 3.9) $\times 10^{-13}$ M in WIN and (0.4 – 2.9) $\times 10^{-13}$ M in SUM, with WIN having higher values than SUM at the same concentration factor (Fig. 2c). $[^{3}C^*]_{PTA}$ is lower than $[^{3}C^*]_{SYR}$ in every dilution, with an average $[^{3}C^*]_{PTA}/[^{3}C^*]_{SYR}$ ratio of 0.67 (±0.22) in WIN and 0.36 (±0.09) in SUM. Since PTA appears to only capture highly oxidizing triplets (Ma et al., 2022), the ratio of $[^{3}C^*]_{PTA}/[^{3}C^*]_{SYR}$ should represent the highly

https://doi.org/10.5194/egusphere-2023-566
Preprint. Discussion started: 28 March 2023

oxidizing fraction of the total oxidizing triplet pool (i.e., 67% in WIN and 36% in SUM). Highly oxidizing ^{3}C* typically are formed from aromatic ketone or carbonyl precursors, such as 3,4-dimethoxybenzaldehyde, while precursors for weakly oxidizing ^{3}C* include polycyclic aromatic structures (e.g. 2-acetonaphthone) (McNeill and Canonica, 2016). Our oxidizing triplet concentrations are approximately 100 times higher than [$^\bullet$OH] (Fig. 2), indicating the likely importance of ^{3}C* as an oxidant in atmospheric drops and particles.

For both probes, the ^{3}C* concentration initially increases with DOC but then approaches or reaches a plateau under more concentrated conditions. Kaur et al. (2019) observed the same trend. Their interpretation was that in dilute solutions O_2 is the dominant sink for triplets, while under more concentrated conditions DOM becomes the major sink. Therefore, ^{3}C* production and loss are both functions of DOC, as described by

$$[^3C^*] = \frac{a[DOC]}{1 + b[DOC]} \quad (11)$$

The dashed lines in Figs. 2b and 2c show the regression fitting results of Equation 11 to the experimental data. From the fitted parameter b (Table S9), we can determine $k_{rxn+Q,3C^*}$ (Eqn. S6), the total rate constant of triplet physical quenching and chemical reaction with DOC. Values from our Fig. 2 fittings are 7.6 (± 6.8) ×10^7 L (mol C)$^{-1}$ s^{-1} for WIN and 1.2 (±0.5) ×10^8 L (mol C)$^{-1}$ s^{-1} for SUM (Table S10). Kaur et al. (2019) obtained 9.3 (±1.3) ×10^7 L (mol C)$^{-1}$ s^{-1} for Davis winter particle extracts, but they did not correct for SYR inhibition, which should be more significant at higher DOC, leading to an earlier plateau and higher apparent rate constant. Despite this, the three values are not significantly different, possibly because the Kaur samples had much lower DOC and thus were less affected by SYR inhibition. Wenk et al. (2013) obtained a range of values of (1.3 – 3.9) ×10^7 L (mol C)$^{-1}$ s^{-1} for surface water DOM quenching and reacting with 2-acetonaphthone and 3-methoxyacetophenone triplets; their lower values imply that atmospheric DOM, at least in our samples, more efficiently quenches triplets than does DOM in surface waters.

The DOC quenching and reaction rate constants from our PTA-derived triplet concentrations are 5.7 (±1.2) ×10^7 and 6.6 (±1.0) ×10^7 L (mol C)$^{-1}$ s^{-1} for WIN and SUM, respectively. These values are lower than those obtained using SYR, as reflected by the weaker curvature of the PTA dashed lines (Figure 2c) compared to SYR (Figure 2b). The similar values of $k_{rxn+Q,3C^*}$ from PTA in WIN and SUM suggest that this rate constant is insensitive to particle type. Therefore, the higher $[^3C^*]_{PTA}$ in WIN compared to SUM at the same DOC level can be attributed

https://doi.org/10.5194/egusphere-2023-566
Preprint. Discussion started: 28 March 2023

to differences in $^3C^*$ production. This is consistent with the differences in apparent quantum yields: the WIN yield of triplets is 1.8 (±0.3)%, more than double the SUM value of 0.8 (±0.1)% (Table S6).

3.3.3 Singlet molecular oxygen in PM extracts

The final photooxidant we measured is singlet molecular oxygen. As shown in Fig. 2d, winter and summer samples have similar $^1O_2^*$ concentrations, in the range of (0.2 – 8.5) $\times 10^{-12}$ M, with values increasing with DOC. The lowest values, in the most dilute extracts, are comparable to fog water concentrations, while our highest concentrations are approximately four times higher than those in previous Davis winter particle extracts (Anastasio and McGregor, 2001; Kaur and Anastasio, 2017; Kaur et al., 2019). $^1O_2^*$ is the most abundant oxidant in our PMEs, with concentrations roughly 10 times higher than $^3C^*$ and 1000 times higher than $^\bullet$OH. In both series of samples, the $^1O_2^*$ concentration increases with DOC, as seen in Kaur et al. (2019). Since brown carbon is the source of $^1O_2^*$, the $^1O_2^*$ production rate increases with DOC. In contrast, in dilute samples (e.g., our extracts) the dominant sink for $^1O_2^*$ is water, whose concentration is independent of sample concentration factor. All three sets of samples in Fig. 2d exhibit very similar relationships between $^1O_2^*$ and DOC, suggesting DOC concentration might be a good predictor of $^1O_2^*$ concentrations in atmospheric waters. Apparent quantum yields of $^1O_2^*$ are 3.0 (± 0.2)% for WIN and 2.0 (± 0.4)% for SUM (Table S8), which are in the range of typical values for atmospheric waters (Bogler et al., 2022; Kaur and Anastasio, 2017; Kaur et al., 2019; Manfrin et al., 2019) and surface waters (Ossola et al., 2020). For WIN, $^1O_2^*$ is linearly related to DOC throughout the dilution series, but in SUM the singlet oxygen concentration exhibits a linear relationship at low DOC and then starts to level off in the more concentrated extracts (Fig. 2d). Kaur et al. (2019) predicted this plateauing under aerosol liquid water conditions as the very high concentration of organics can become the dominant $^1O_2^*$ sink. However, a better explanation for this curvature in our samples is that the concentration of $^3C^*$ (the precursor of $^1O_2^*$) plateaus at high DOC, which slows the production rate of $^1O_2^*$. In the summer sample of Figure 2d, the curvature of $^1O_2^*$ is more likely a consequence of $^3C^*$ plateauing, rather than DOC becoming an important $^1O_2^*$ sink, because $^1O_2^*$ generally has lower reactivity than triplets with most organics (Arnold, 2014; Canonica et al., 2000; Wilkinson et al., 1995). Based on rough estimates of the composition and reactivity of particulate organics from biomass burning (Kaur et al., 2019), we estimate that for organics to be an important sink of $^1O_2^*$, the DOC concentration would need to be ~5000 mg C L^{-1}; this is 10 times higher than the maximum DOC in our extracts, suggesting that organics are a negligible sink of $^1O_2^*$ in our extracts. Assuming $^3C^*$ is responsible for the $^1O_2^*$ curvature in the

https://doi.org/10.5194/egusphere-2023-566
Preprint. Discussion started: 28 March 2023

SUM sample, we can derive a kinetic equation for [$^1O_2$*] as a function of DOC, taking the plateauing ^{3}C* concentration into consideration. The simplified equation, Eq. S8, is analogous to Eq. 11 and is derived in Section S2.

This equation gives a good fit to the SUM data, as shown by the red dashed line in Fig. 2d. From the parameter *b*, we calculate that the rate constant for DOC reacting and physically quenching $^1O_2$*-producing triplet states ($k_{rxn+Q,3C*}$) is 2.1 (± 0.3) ×10^7 L (mol C)$^{-1}$ s^{-1}. This is lower than the values acquired from [^{3}C*]$_{SYR}$ and [^{3}C*]$_{PTA}$, which is reasonable since the $^1O_2$*-derived value represents the whole triplet pool (i.e., all triplets that can undergo energy transfer with dissolved oxygen), which is a larger pool than oxidizing triplets. Our results suggest that the non-oxidizing triplets are less reactive with organics than are oxidizing triplets, leading to a lower rate constant for reaction and quenching by DOC, as seen previously by Canonica et al. (2000).

3.4 Extrapolating photooxidant concentrations to ALW conditions

In the dilution experiments above, we investigate oxidant kinetics and concentrations as a function of concentration factor, i.e., particle mass/water mass ratio. In this section we extrapolate these relationships from our dilute extract conditions (with PM mass/water mass ratios of (0.04 – 1.6) × 10^{-3} µg PM/µg H_2O) to the much more concentrated conditions of aerosol liquid water (up to ~ 1 µg PM/µg H_2O).

3.4.1 Hydroxyl radical in ALW

To estimate [•OH] in particle water for WIN, we apply the linear relationships of P_{OH} and k'_{OH} with DOC that we determined in our extracts (Fig. 3a), along with the relationship of [DOC] to particle mass/water mass ratio, to predict kinetics under more concentrated particle water conditions. Parameters used in the extrapolation are provided in Table S11. Extrapolating to an ALW of 1 µg PM/µg H_2O yields an estimated P_{OH} of 2.7 ×10^{-5} M s^{-1}, and k'_{OH} of 5.0 × 10^9 s^{-1}. However, since our aqueous experiments do not include •OH transferred from the gas phase ($P_{OH,gas}$), we added $P_{OH,gas}$ estimated by Kaur et al. (2019) to our extrapolated P_{OH} to calculate $P_{OH,tot}$. We then estimate [•OH] as $P_{OH,tot}$ divided by k'_{OH} (Eq. 10). Estimating [•OH] for the SUM sample is more complicated since P_{OH} initially increases with DOC squared. We simulate the •OH production rate as a function of DOC by using photo-Fenton reaction rate constants and setting soluble iron and hydrogen peroxide concentrations to fit measured values (Section S3). We then apply this simple model to predict P_{OH} for SUM out to ALW conditions. For k'_{OH} in SUM, we use the measured linear dependence on DOC (Fig. 3b).

https://doi.org/10.5194/egusphere-2023-566
Preprint. Discussion started: 28 March 2023

Figure 4a shows the predicted hydroxyl radical steady-state concentrations for SUM and WIN across a wide range of liquid water content, from dilute cloud/fog drops to concentrated aqueous particle conditions. We also include the winter PM •OH predictions from Kaur et al. (2019) for comparison. For WIN, [•OH] slowly decreases from 1×10^{-14} M in cloud/fog waters (at 3×10^{-5} µg PM/µg H_2O) to 6×10^{-15} M in ALW (at 1 µg PM/µg H_2O). Calculated [•OH] values are higher than measured values, especially under the most dilute conditions, because •OH from gas-phase mass transfer is included in our extrapolation. The •OH trend for WIN is consistent with the result of Kaur et al. (2019), but our concentrations are 6 – 12 times higher. This is because WIN has a slope of P_{OH} vs. DOC around 4 times higher than that in Kaur et al. (2019), while the slope for k'_{OH} in WIN is slightly lower (Fig. 3a). For our winter sample under dilute conditions, aqueous processes are as important an •OH source as is gas-phase transfer (Fig. 4b). However, the aqueous production rate rises more rapidly with PM mass concentration than does gas-phase mass transfer, making aqueous reactions the dominant source of •OH under ALW conditions, where they account for more than 90% of •OH production. This slower increase of $P_{OH,gas}$ is also responsible for the decreasing [•OH] with increasing PM mass concentration.

For SUM, predicted [•OH] is approximately constant at 4×10^{-15} M under dilute conditions (Fig. 4a), with gas-phase mass transport being the major source of •OH (Fig. 4c). [•OH] then increases to 1×10^{-14} M at 1×10^{-3} µg PM/µg H_2O as the aqueous production rate ($P_{OH,aq}$) increases rapidly and aqueous reactions dominate •OH production. When moving to more concentrated conditions, [•OH] plateaus because we assume the aqueous H_2O_2 concentration reaches a maximum of 100 µM due to equilibrium with the gas phase (Section S3). Thereafter, $P_{OH,aq}$ increases linearly, but more slowly, with PM mass/water mass ratio; since k'_{OH} also increases linearly with concentration factor, [•OH] remains nearly constant at 9×10^{-15} M for PM/water ratios of roughly 10^{-3} to 1 µg PM/µg H_2O. For both WIN and SUM, our measured •OH concentrations in the most concentrated extracts are approximately an order of magnitude higher than in Kaur et al. (2019) and this difference is maintained throughout the predicted [•OH] to ambient particle water conditions.

https://doi.org/10.5194/egusphere-2023-566
Preprint. Discussion started: 28 March 2023

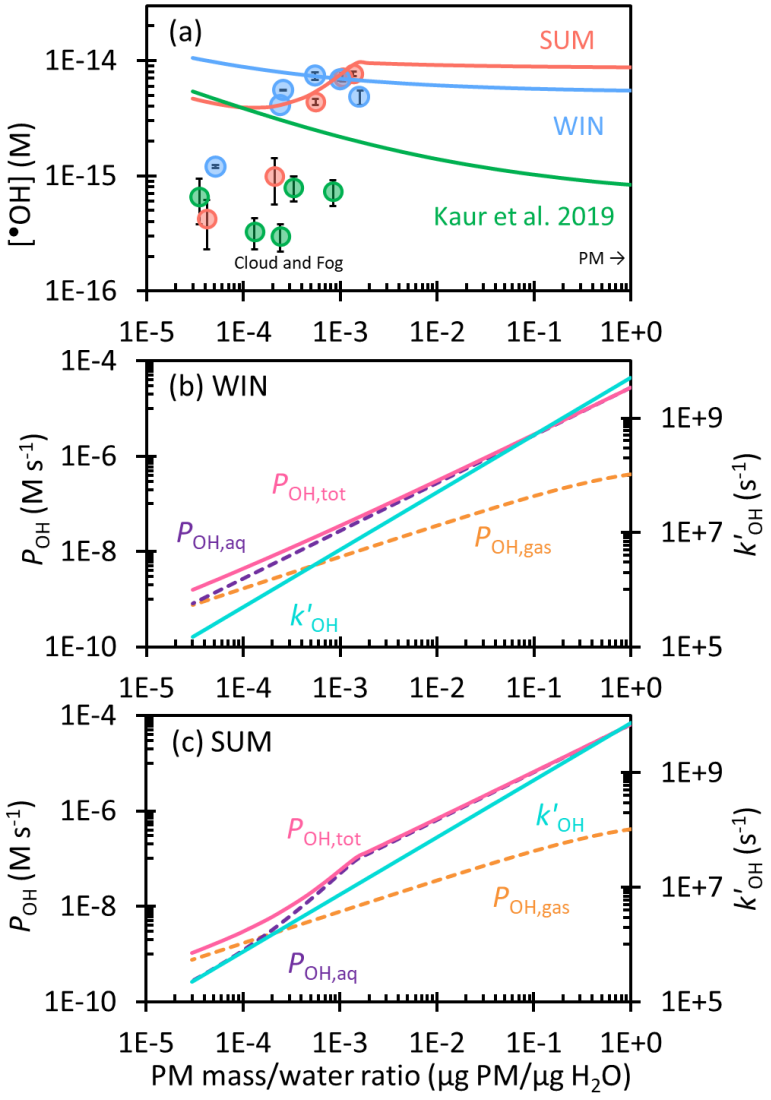

Figure 4. (a) Dependence of hydroxyl radical concentration on particle mass/water mass ratio in winter (blue) and summer (red) extracts. Solid circles are measured values, while lines are extrapolations to the ambient aqueous aerosol conditions, including contributions from aqueous •OH formation and •OH mass transport from the gas phase. 490 **Previous measurements and extrapolation with Davis winter particle extracts are shown in green (Kaur et al., 2019). (b) & (c) Dependence of hydroxyl radical production rate, including the rate of transport from the gas phase ($P_{OH,gas}$, orange), aqueous reaction ($P_{OH,aq}$, purple), and the total rate ($P_{OH,tot}$ = $P_{OH,aq}$ + $P_{OH,gas}$, pink), and the rate constant of •OH loss by natural sinks (k'_{OH}, blue) on particle mass/water mass ratio for (b) WIN and (c) SUM.**

https://doi.org/10.5194/egusphere-2023-566
Preprint. Discussion started: 28 March 2023

3.4.2 Oxidizing triplet concentrations in ALW

To predict $^3C^*$ concentrations in aerosol liquid water, we used the data in Table S11 to extrapolate $^3C^*$ production rates (P_{3C^*}) and sinks (k'_{3C^*}) to concentrated conditions and calculated $^3C^*$ concentrations for SYR and PTA with Eq.10. As shown in Figs. 5a and 5b, measured [$^3C^*$] in SUM and WIN are higher than the results in Kaur et al. (2019) at the same particle mass/water ratio. This is likely due to higher ratios of OC/PM in our samples. In all three sets of samples, [$^3C^*$] rises rapidly with PM mass/water mass ratio at low DOC, and then reaches or approaches a plateau under aqueous aerosol conditions, as the dominant triplet sink transitions from dissolved O_2 to DOC. We believe the production rate of $^3C^*$ linearly increases with particle mass/water mass ratio (P_{3C^*} in Figs. 5c and 5d), but the sinks for triplets change, as proposed by Kaur et al. (2019): under dilute conditions, O_2 is a dominant and constant sink ($k'_{3C^*,O2}$), causing [$^3C^*$] to increase with increasing concentration factor. For our more concentrated extracts (and continuing at higher PM mass/water mass ratios), organic compounds become the major sink for $^3C^*$ (Figs. 5c and d). Thus the ratio of the production rate and sink rate constant becomes constant at higher DOC, causing [$^3C^*$] to plateau. For SYR, we predict WIN and SUM both reach a maximum value of 8×10^{-13} M at 1 µg PM/µg H_2O. This value is 22 times higher than the concentration under the most dilute conditions in WIN and around 8 times higher than the dilute result in SUM. While SUM starts with a higher $[^3C^*]_{SYR}$ under dilute conditions, it experiences greater curvature than WIN, apparently because its organic compounds react with and/or physically quench oxidizing triplets more rapidly (i.e., $k'_{3C^*,DOC}$ is larger for SUM than WIN). For both samples, the ALW prediction for $[^3C^*]_{SYR}$ is near the geometric mean of the two bounding fits of Kaur et al. (2019). For the lower $^3C^*$ concentrations determined by PTA, SUM and WIN start with essentially the same $[^3C^*]_{PTA}$, 3×10^{-14} and 2×10^{-14} M, respectively, at 3×10^{-5} µg PM/µg H_2O. SUM exhibits more curvature, as seen for $[^3C^*]_{SYR}$, leading to a lower predicted $[^3C^*]_{PTA}$ at 1 µg PM/µg H_2O: 4×10^{-13} M for SUM vs. 6×10^{-13} M for WIN. $[^3C^*]_{PTA}$ increases by factors of 14 and 29 for SUM and WIN, respectively, from the most dilute condition to ALW condition, similar to $[^3C^*]_{SYR}$.

https://doi.org/10.5194/egusphere-2023-566
Preprint. Discussion started: 28 March 2023

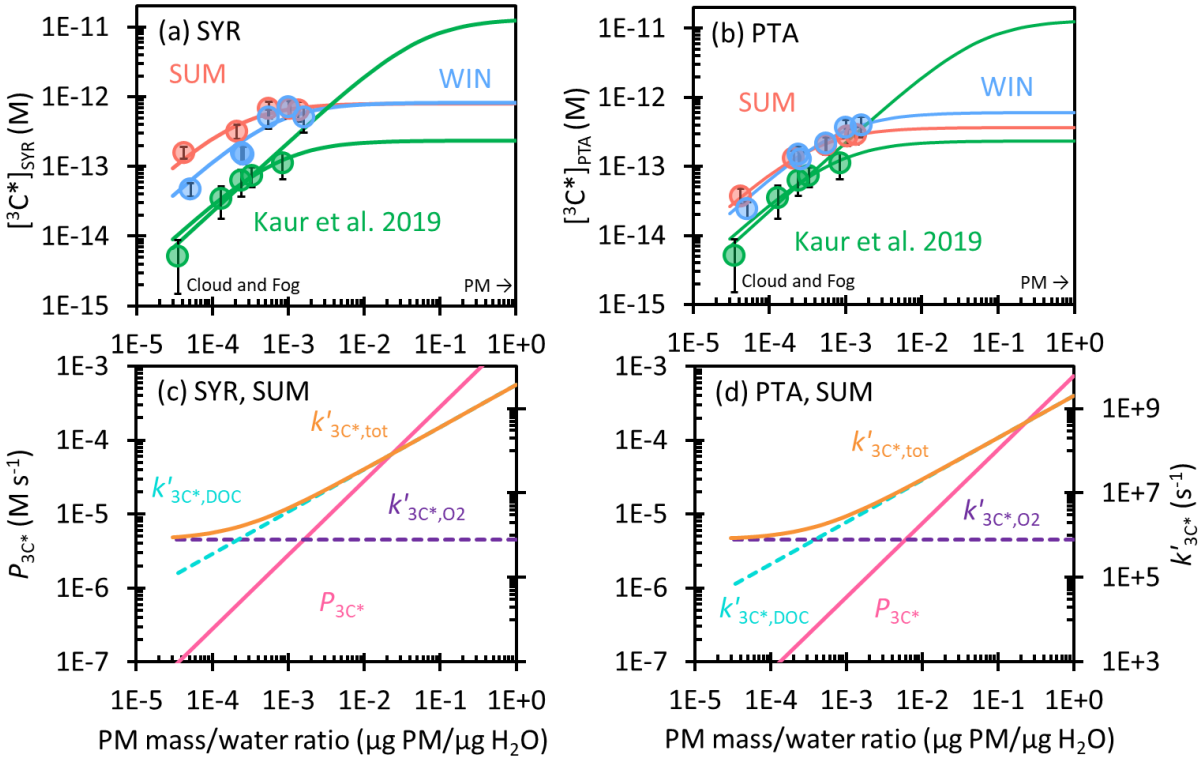

Figure 5. Top row: Dependence of triplet excited state concentration determined by (a) SYR and (b) PTA on particle mass/water mass ratio in WIN (blue) and SUM (red). Solid circles are measured values in dilution experiments, while lines are extrapolations to ALW conditions. Previous measurements and extrapolations (best fit and high estimate) for Davis winter particle extracts are in green (Kaur et al., 2019). Bottom row: Triplet production rate ($P_{^3C^*}$, pink line) and first-order rate constants for $^3C^*$ loss, including quenching by oxygen ($k'_{^3C^*,O_2}$, dashed purple), dissolved organic carbon ($k'_{^3C^*,DOC}$, dashed blue), and total ($k'_{^3C^*,tot} = k'_{^3C^*,O_2} + k'_{^3C^*,DOC}$, orange) determined by (c) SYR and (d) PTA for SUM. Figure S4 shows $P_{^3C^*}$ and $k'_{^3C^*}$ for WIN.

3.4.3 Singlet molecular oxygen in ALW

Lastly, we consider the extrapolation of $^1O_2^*$ concentrations from our dilute experimental solutions to ALW conditions. To do this, we consider the production of $^1O_2^*$ by $^3C^*$ as well as H_2O and DOM as sinks for singlet oxygen. In terms of $^1O_2^*$ sources, we first assume the O_2 concentration is constant at all conditions, i.e., not considering a solute effect on O_2 solubility. Next, we assume the plateauing of $[^3C^*]$ at high concentration factors results in a plateauing of the $^1O_2^*$ production rate, as evidenced in the curvature of $[^1O_2^*]$ in SUM (Fig. 2d). To

https://doi.org/10.5194/egusphere-2023-566
Preprint. Discussion started: 28 March 2023

account for this effect, we fit [$^1O_2$*] versus DOC using an equation analogous to Eq. 11 and calculate the $^1O_2$* production rate (P_{1O2*}) with the fitted parameters (Eq. S11). This process does not work for WIN, however, since it shows no curvature of [$^1O_2$*]. So to predict the ^{3}C* effect for this sample, we adjusted the regression parameters so that the fitted line passed through just the first four data points (Figure S5). In terms of modeling DOM as a sink for $^1O_2$*, this effect does not appear in our lab extracts (due to their relatively low DOC content), but we expect it will happen under more concentrated conditions. To incorporate this effect, we estimated the second-order rate constant for loss of $^1O_2$* by DOC ($k_{1O2*+DOC}$) using the same approach from Kaur et al. (2019) but determined a lower value (1×10^5 L (mol C)$^{-1}$ s^{-1}) based on our $^1O_2$* concentration data versus DOC . We then calculate the first-order sink for $^1O_2$* due to DOC as the product of this second-order rate constant and the DOC concentration.

https://doi.org/10.5194/egusphere-2023-566
Preprint. Discussion started: 28 March 2023

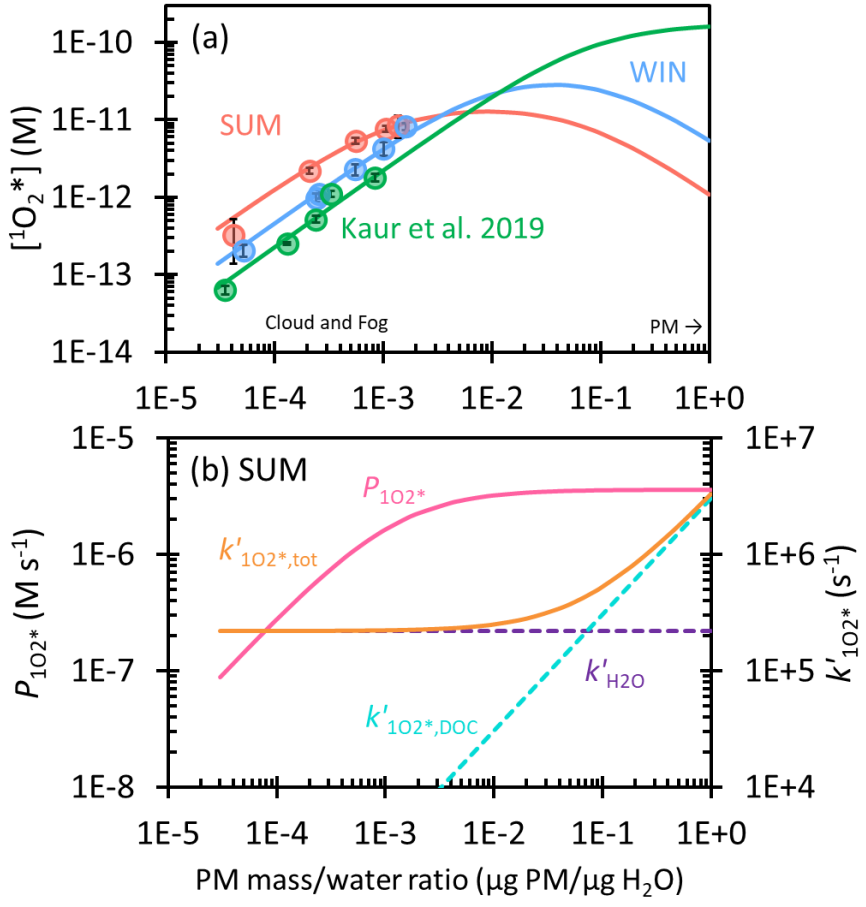

Figure 6. (a) Dependence of singlet molecular oxygen concentration on particle mass/water mass ratio in winter (blue) and summer (red) samples. Solid circles are measured values in dilution experiments, while lines are extrapolations to ALW conditions. Previous measurements and extrapolation with Davis winter particle extracts are in green (Kaur et al., 2019). (b) Dependence of singlet oxygen production rate ($P_{^1O_2^*}$, pink line) and the rate constant for $^1O_2^*$ loss, including deactivation by water (k'_{H2O}, dashed purple), quenching by dissolved organic carbon ($k'_{^1O_2^*,DOC}$, dashed blue), and the total sink ($k'_{^1O_2^*,tot} = k'_{H2O} + k'_{^1O_2^*,DOC}$, orange) on particle mass/water mass ratio for SUM. Figure S6 shows $P_{^1O_2^*}$ and $k'_{^1O_2^*}$ for the winter sample.

The resulting predictions for $^1O_2^*$ concentrations, along with the production rate and sink rate constants for the summer sample, are in Figure 6. Figure 6a shows that our predictions of $^1O_2^*$ under ALW conditions are roughly 10 to 100 times lower than those in Kaur et al. (2019); this is because we include the effect of plateauing $^3C^*$ concentration on the $^1O_2^*$ production rate, which decreases $^1O_2^*$ concentrations under ALW conditions. In Fig.

https://doi.org/10.5194/egusphere-2023-566
Preprint. Discussion started: 28 March 2023

6a, [$^1O_2$*] for SUM starts at 4 × 10^{-13} M in dilute drops, peaks at 1 ×10^{-11} M at 1.0 ×10^{-2} µg PM/µg H_2O (where P_{1O2*} first plateaus; Fig. 6b), and then starts to decrease. This decrease is because the production rate for $^1O_2$* (P_{1O2*}) is constant while the $^1O_2$* sink from DOC ($k'_{1O2*,DOC}$) increases with particle mass concentration and becomes the dominant $^1O_2$* sink; the result is a singlet oxygen concentration of 1 × 10^{-12} M at 1 µg PM/µg H_2O. This concentration is only 1.4 times higher than $[^3C^*]_{SYR}$ under the same condition (Fig. S7). For WIN, [$^1O_2$*] starts at 1 ×10^{-13} M in dilute drops, reaches a maximum of 3 × 10^{-11} M at 4.0 ×10^{-2} µg PM/µg H_2O, and then decreases to 5 ×10^{-12} M at 1 µg PM/µg H_2O (Fig. S6). Under ALW conditions, WIN has a maximum [$^1O_2$*] that is 3 times higher than SUM because measured [$^1O_2$*] in WIN presents much less curvature than SUM, i.e., the organics in WIN appear to be less reactive with $^1O_2$*-producing triplet states compared to those in the SUM sample. Therefore, the plateau of P_{1O2*} in WIN shows up only under more concentrated conditions compared to SUM (Fig. S6).

Conclusions and uncertainties

We measured concentrations of three photooxidants - hydroxyl radical, oxidizing triplet excited states of organic matter, and singlet molecular oxygen - as a function of particle dilution in aqueous extracts of winter particles (influenced by residential wood combustion) and summer particles (strongly influenced by wildfires). The extracts contain high amounts of organic matter, with dissolved organic carbon concentrations ranging from 10 to 495 mg C L^{-1}. DOC-normalized mass absorption coefficients at 300 nm are 2.1 (±0.2) m^2 (g C)$^{-1}$ in winter and 3.1 (±0.1) m^2 (g C)$^{-1}$ in summer, with absorption Ångström exponents of 7.2 for both, indicating significant amounts of brown carbon.

In the winter sample, the measured $^{\bullet}$OH concentration appears to be independent of extract concentration, while in the summer sample $^{\bullet}$OH increases with concentration factor. In both WIN and SUM, measured $^3C^*$ concentrations determined by our two probes initially increase rapidly with concentration factor, then approach or reach a plateau under more concentrated conditions. Measured $^1O_2$* concentrations in WIN are linear with DOC, while in SUM singlet oxygen levels show curvature (like $^3C^*$) in more concentrated extracts. By extrapolating the oxidant kinetics in our dilute extracts to the much more concentrated conditions of ambient particle water (1 µg PM/µg H_2O), we obtain photooxidant concentrations of [$^{\bullet}$OH] = (6 – 9) × 10^{-15} M, [$^3C^*$] = (4 – 8) × 10^{-13} M, and [$^1O_2$*] = (1 – 5) × 10^{-12} M. The $^{\bullet}$OH particle water concentrations are not significantly different from those in fog/cloud waters, while [$^3C^*$] and [$^1O_2$*] are 10 – 30 and 3 – 40 times higher, respectively, than

https://doi.org/10.5194/egusphere-2023-566
Preprint. Discussion started: 28 March 2023

fog/cloud values (at 3×10^{-5} µg PM/µg H_2O). The ratio of concentrations of $^1O_2$*: ^{3}C*: $^{\bullet}$OH in aerosol liquid water is $10^3 – 10^2 : 10^2 : 1$, which is lower than the $10^5 : 10^4 – 10^2$: 1 ALW ratio predicted by Kaur et al. (2019). This is because our predicted ALW concentration of $^{\bullet}$OH is approximately 10 times higher than in the past work, while ^{3}C* is around 5 times higher than their best fit, and $^1O_2$* is 30 – 150 times lower than their prediction (Fig. S7). Kaur et al. (2019) discussed the large uncertainties in predicting $^1O_2$* and ^{3}C* for ALW conditions, in part because of the difficulty experimentally observing the interactions between DOC and ^{3}C* or $^1O_2$*. However, in this current work, we are able to clearly see triplet quenching by DOC since organic carbon concentrations in our particle water extracts were up to 5 times higher than in the past work. When extrapolating to more concentrated conditions, we predict ^{3}C* concentrations are heavily suppressed due to quenching by DOC, resulting in triplet concentrations that are between the two estimates from Kaur et al. (2019). For the first time, we also see curvature in [$^1O_2$*] versus DOC in our most concentrated summer extracts, which appears to result from suppression of triplets by organics. With this experimental finding, we are able to include this effect in the prediction of $^1O_2$* concentrations under particle water conditions.

While our samples have higher DOC than the dilution sample in Kaur et al. (2019), our extrapolations from dilute extracts to ALW still span a huge range (approximately a factor of 600 in PM mass/water mass ratio), bringing significant uncertainties. For example, it is unclear whether an appreciable portion of the organic compounds will precipitate under the much more concentrated conditions of ALW. In terms of experimental uncertainties, we could not observe how efficiently organic matter quenches $^1O_2$* and thus were only able to estimate an upper bound of the rate constant, which is poorly constrained. In addition, highly concentrated particle extracts make it difficult to measure ^{3}C* by SYR because of strong inhibition by dissolved organic matter, with inhibition corrections up to a factor of 7.5 in our samples. Additionally, the difficulty in inhibition factor measurements (and resulting high uncertainties) in concentrated extracts can bring large uncertainties. High DOC concentrations also result in significant light screening, which carries additional uncertainty in the corresponding correction. While future work could use more concentrated particle extracts to reduce the extrapolation uncertainty, this approach would likely increase other uncertainties, including light screening and probe inhibition. Also, it is unlikely that the bulk solution approach that we have used can ever approach the concentration conditions in particle water. Because of this, other approaches, such as flow tubes or reaction chambers, will be required to more closely simulate oxidant generation and subsequent reactions in ambient aerosols.

https://doi.org/10.5194/egusphere-2023-566
Preprint. Discussion started: 28 March 2023

Data availability

All data are available upon request.

Author contribution

CA and LM developed the research goals and designed the experiments. KB lent and set up the PM sampler, while LM and CG collected samples. LM and RL performed the photochemistry experiments while WJ and CN analyzed OC and ions, respectively. LM analyzed the data and prepared the manuscript with contributions from all co-authors. CA reviewed, wrote portions of, and edited the manuscript. CA and QZ provided supervision and oversight during the experiments and writing.

Competing interests

The authors declare that they have no conflict of interest.

Financial support

This research has been supported by the National Science Foundation (grants 1649212 and 2220307); the California Agricultural Experiment Station (Projects CA-D-LAW-6403-RR and CA-D-ETX-2102-H); and the University of California, Davis (Donald G. Crosby Graduate Fellowship in Environmental Chemistry and Jastro Shields Research Awards).

https://doi.org/10.5194/egusphere-2023-566
Preprint. Discussion started: 28 March 2023

References

Anastasio, C. and McGregor, K. G.: Chemistry of fog waters in California's Central Valley: 1. In situ photoformation of hydroxyl radical and singlet molecular oxygen, Atmos. Environ., 35(6), 1079–1089, doi:10.1016/S1352-2310(00)00281-8, 2001.

Anastasio, C. and Newberg, J. T.: Sources and sinks of hydroxyl radical in sea-salt particles, J. Geophys. Res., 112(D10), doi:10.1029/2006JD008061, 2007.

Andreae, M. O.: Soot carbon and excess fine potassium: long-range transport of combustion-derived aerosols., Science, 220(4602), 1148–1151, doi:10.1126/science.220.4602.1148, 1983.

Appiani, E., Ossola, R., Latch, D. E., Erickson, P. R. and McNeill, K.: Aqueous singlet oxygen reaction kinetics of furfuryl alcohol: effect of temperature, pH, and salt content, Environ. Sci.: Processes Impacts, 19(4), 507–516, doi:10.1039/C6EM00646A, 2017.

Arakaki, T., Anastasio, C., Kuroki, Y., Nakajima, H., Okada, K., Kotani, Y., Handa, D., Azechi, S., Kimura, T., Tsuhako, A. and Miyagi, Y.: A general scavenging rate constant for reaction of hydroxyl radical with organic carbon in atmospheric waters., Environ. Sci. Technol., 47(15), 8196–8203, doi:10.1021/es401927b, 2013.

Arakaki, T. and Faust, B. C.: Sources, sinks, and mechanisms of hydroxyl radical (˙OH) photoproduction and consumption in authentic acidic continental cloud waters from Whiteface Mountain, New York: The role of the Fe(r) (r = II, III) photochemical cycle, J. Geophys. Res., 103(D3), 3487–3504, doi:10.1029/97JD02795, 1998.

Arciva, S., Niedek, C., Mavis, C., Yoon, M., Sanchez, M. E., Zhang, Q. and Anastasio, C.: Aqueous ·OH oxidation of highly substituted phenols as a source of secondary organic aerosol., Environ. Sci. Technol., 56(14), 9959–9967, doi:10.1021/acs.est.2c02225, 2022.

Arnold, W. A.: One electron oxidation potential as a predictor of rate constants of N-containing compounds with carbonate radical and triplet excited state organic matter., Environ. Sci. Process. Impacts, 16(4), 832–838, doi:10.1039/c3em00479a, 2014.

Ashton, L., Buxton, G. V. and Stuart, C. R.: Temperature dependence of the rate of reaction of OH with some aromatic compounds in aqueous solution. Evidence for the formation of a π-complex intermediate?, J. Chem. Soc., Faraday Trans., 91(11), 1631–1633, doi:10.1039/FT9959101631, 1995.

Badali, K. M., Zhou, S., Aljawhary, D., Antiñolo, M., Chen, W. J., Lok, A., Mungall, E., Wong, J. P. S., Zhao, R. and Abbatt, J. P. D.: Formation of hydroxyl radicals from photolysis of secondary organic aerosol material, Atmos. Chem. Phys., 15(14), 7831–7840, doi:10.5194/acp-15-7831-2015, 2015.

https://doi.org/10.5194/egusphere-2023-566
Preprint. Discussion started: 28 March 2023

Bilski, P., Holt, R. N. and Chignell, C. F.: Properties of singlet molecular oxygen in binary solvent mixtures of different polarity and proticity, J. Photochem. Photobiol. A, 109(3), 243–249, doi:10.1016/S1010-6030(97)00147-0, 1997.

Bogler, S., Daellenbach, K. R., Bell, D. M., Prévôt, A. S. H., El Haddad, I. and Borduas-Dedekind, N.: Singlet oxygen seasonality in aqueous PM10 is driven by biomass burning and anthropogenic secondary organic aerosol, Environ. Sci. Technol., doi:10.1021/acs.est.2c04554, 2022.

Canonica, S. and Freiburghaus, M.: Electron-rich phenols for probing the photochemical reactivity of freshwaters., Environ. Sci. Technol., 35(4), 690–695, doi:10.1021/es0011360, 2001.

Canonica, S., Hellrung, B. and Wirz, J.: Oxidation of phenols by triplet aromatic ketones in aqueous solution, The Journal of Physical Chemistry A, 104(6), 1226–1232, 2000.

Canonica, S. and Laubscher, H.-U.: Inhibitory effect of dissolved organic matter on triplet-induced oxidation of aquatic contaminants, Photochem. Photobiol. Sci., 7(5), 547, doi:10.1039/b719982a, 2008.

Chellamani, A. and Sengu, P.: Mechanistic study on the oxidation of (phenylthio)acetic acids by oxo(salen)manganese(V) complexes and the reactivity–selectivity principle, J. Mol. Catal. A: Chem, 283(1-2), 83–92, doi:10.1016/j.molcata.2007.12.004, 2008.

Ervens, B.: Progress and problems in modeling chemical processing in cloud droplets and wet aerosol particles, in Multiphase environmental chemistry in the atmosphere, vol. 1299, edited by S. W. Hunt, A. Laskin, and S. A. Nizkorodov, pp. 327–345, American Chemical Society, Washington, DC., 2018.

Ervens, B., Sorooshian, A., Lim, Y. B. and Turpin, B. J.: Key parameters controlling OH-initiated formation of secondary organic aerosol in the aqueous phase (aqSOA), J. Geophys. Res. Atmos., 119(7), 3997–4016, doi:10.1002/2013JD021021, 2014.

Ervens, B., Turpin, B. J. and Weber, R. J.: Secondary organic aerosol formation in cloud droplets and aqueous particles (aqSOA): a review of laboratory, field and model studies, Atmos. Chem. Phys., 11(21), 11069–11102, doi:10.5194/acp-11-11069-2011, 2011.

Ervens, B. and Volkamer, R.: Glyoxal processing by aerosol multiphase chemistry: towards a kinetic modeling framework of secondary organic aerosol formation in aqueous particles, Atmos. Chem. Phys., 10(17), 8219–8244, doi:10.5194/acp-10-8219-2010, 2010.

Faust, B. C. and Allen, J. M.: Aqueous-phase photochemical sources of peroxyl radicals and singlet molecular oxygen in clouds and fog, J. Geophys. Res., 97(D12), 12913, doi:10.1029/92JD00843, 1992.

Faust, B. C. and Allen, J. M.: Aqueous-phase photochemical formation of hydroxyl radical in authentic cloudwaters and fogwaters, Environ. Sci. Technol., 27(6), 1221–1224, doi:10.1021/es00043a024, 1993.

https://doi.org/10.5194/egusphere-2023-566
Preprint. Discussion started: 28 March 2023

Faust, J. A., Wong, J. P. S., Lee, A. K. Y. and Abbatt, J. P. D.: Role of aerosol liquid water in secondary organic aerosol formation from volatile organic compounds., Environ. Sci. Technol., 51(3), 1405–1413, doi:10.1021/acs.est.6b04700, 2017.

Fleming, L. T., Lin, P., Roberts, J. M., Selimovic, V., Yokelson, R., Laskin, J., Laskin, A. and Nizkorodov, S. A.: Molecular composition and photochemical lifetimes of brown carbon chromophores in biomass burning organic aerosol, Atmos. Chem. Phys., 20(2), 1105–1129, doi:10.5194/acp-20-1105-2020, 2020.

Forrister, H., Liu, J., Scheuer, E., Dibb, J., Ziemba, L., Thornhill, K. L., Anderson, B., Diskin, G., Perring, A. E., Schwarz, J. P., Campuzano-Jost, P., Day, D. A., Palm, B. B., Jimenez, J. L., Nenes, A. and Weber, R. J.: Evolution of brown carbon in wildfire plumes, Geophys. Res. Lett., 42(11), 4623–4630, doi:10.1002/2015GL063897, 2015.

Galbavy, E. S., Ram, K. and Anastasio, C.: 2-Nitrobenzaldehyde as a chemical actinometer for solution and ice photochemistry, J. Photochem. Photobiol. A, 209(2-3), 186–192, doi:10.1016/j.jphotochem.2009.11.013, 2010.

Gemayel, R., Emmelin, C., Perrier, S., Tomaz, S., Baboomian, V. J., Fishman, D. A., Nizkorodov, S. A., Dumas, S. and George, C.: Quenching of ketone triplet excited states by atmospheric halides, Environ. Sci.: Atmos., 1(1), 31–44, doi:10.1039/D0EA00011F, 2021.

Gilardoni, S., Massoli, P., Paglione, M., Giulianelli, L., Carbone, C., Rinaldi, M., Decesari, S., Sandrini, S., Costabile, F., Gobbi, G. P., Pietrogrande, M. C., Visentin, M., Scotto, F., Fuzzi, S. and Facchini, M. C.: Direct observation of aqueous secondary organic aerosol from biomass-burning emissions., Proc. Natl. Acad. Sci. USA, 113(36), 10013–10018, doi:10.1073/pnas.1602212113, 2016.

González Palacios, L., Corral Arroyo, P., Aregahegn, K. Z., Steimer, S. S., Bartels-Rausch, T., Nozière, B., George, C., Ammann, M. and Volkamer, R.: Heterogeneous photochemistry of imidazole-2-carboxaldehyde: HO_2 radical formation and aerosol growth, Atmos. Chem. Phys., 16(18), 11823–11836, doi:10.5194/acp-16-11823-2016, 2016.

Haag, W. R., Hoigne´, J., Gassman, E. and Braun, A.: Singlet oxygen in surface waters — Part I: Furfuryl alcohol as a trapping agent, Chemosphere, 13(5-6), 631–640, doi:10.1016/0045-6535(84)90199-1, 1984.

De Haan, D. O., Jansen, K., Rynaski, A. D., Sueme, W. R. P., Torkelson, A. K., Czer, E. T., Kim, A. K., Rafla, M. A., De Haan, A. C. and Tolbert, M. A.: Brown carbon production by aqueous-phase interactions of glyoxal and SO2, Environ. Sci. Technol., 54(8), 4781–4789, doi:10.1021/acs.est.9b07852, 2020.

https://doi.org/10.5194/egusphere-2023-566
Preprint. Discussion started: 28 March 2023

Hecobian, A., Zhang, X., Zheng, M., Frank, N., Edgerton, E. S. and Weber, R. J.: Water-Soluble Organic Aerosol material and the light-absorption characteristics of aqueous extracts measured over the Southeastern United States, Atmos. Chem. Phys., 10(13), 5965–5977, doi:10.5194/acp-10-5965-2010, 2010.

Herrmann, H., Hoffmann, D., Schaefer, T., Bräuer, P. and Tilgner, A.: Tropospheric aqueous-phase free-radical chemistry: radical sources, spectra, reaction kinetics and prediction tools., ChemPhysChem, 11(18), 3796–3822, doi:10.1002/cphc.201000533, 2010.

Herrmann, H., Schaefer, T., Tilgner, A., Styler, S. A., Weller, C., Teich, M. and Otto, T.: Tropospheric aqueous-phase chemistry: kinetics, mechanisms, and its coupling to a changing gas phase., Chem. Rev., 115(10), 4259–4334, doi:10.1021/cr500447k, 2015.

Hoffer, A., Gelencsér, A., Guyon, P., Kiss, G., Schmid, O., Frank, G. P., Artaxo, P. and Andreae, M. O.: Optical properties of humic-like substances (HULIS) in' ' biomass-burning aerosols, Atmos. Chem. Phys., 6(11), 3563–3570, doi:10.5194/acp-6-3563-2006, 2006.

Kaur, R. and Anastasio, C.: Light absorption and the photoformation of hydroxyl radical and singlet oxygen in fog waters, Atmos. Environ., 164, 387–397, doi:10.1016/j.atmosenv.2017.06.006, 2017.

Kaur, R. and Anastasio, C.: First measurements of organic triplet excited states in atmospheric waters., Environ. Sci. Technol., 52(9), 5218–5226, doi:10.1021/acs.est.7b06699, 2018.

Kaur, R., Labins, J. R., Helbock, S. S., Jiang, W., Bein, K. J., Zhang, Q. and Anastasio, C.: Photooxidants from brown carbon and other chromophores in illuminated particle extracts, Atmos. Chem. Phys., 19(9), 6579–6594, doi:10.5194/acp-19-6579-2019, 2019.

Klein, E., Lukeš, V., Cibulková, Z. and Polovková, J.: Study of N–H, O–H, and S–H bond dissociation enthalpies and ionization potentials of substituted anilines, phenols, and thiophenols, Journal of Molecular Structure: THEOCHEM, 758(2-3), 149–159, doi:10.1016/j.theochem.2005.10.015, 2006.

Li, M., Bao, F., Zhang, Y., Sheng, H., Chen, C. and Zhao, J.: Photochemical aging of soot in the aqueous phase: release of dissolved black carbon and the formation of $^1O_2$, Environ. Sci. Technol., 53(21), 12311–12319, doi:10.1021/acs.est.9b02773, 2019.

Lim, Y. B., Tan, Y., Perri, M. J., Seitzinger, S. P. and Turpin, B. J.: Aqueous chemistry and its role in secondary organic aerosol (SOA) formation, Atmos. Chem. Phys., 10(21), 10521–10539, doi:10.5194/acp-10-10521-2010, 2010.

Lin, G., Sillman, S., Penner, J. E. and Ito, A.: Global modeling of SOA: the use of different mechanisms for aqueous-phase formation, Atmos. Chem. Phys., 14(11), 5451–5475, doi:10.5194/acp-14-5451-2014, 2014.

https://doi.org/10.5194/egusphere-2023-566
Preprint. Discussion started: 28 March 2023

Ma, L., Guzman, C., Niedek, C., Tran, T., Zhang, Q. and Anastasio, C.: Kinetics and mass yields of aqueous secondary organic aerosol from highly substituted phenols reacting with a triplet excited state, Environ. Sci. Technol., 55(9), 5772–5781, doi:10.1021/acs.est.1c00575, 2021.

Ma, L., Worland, R., Tran, T. and Anastasio, C.: An evaluation of probes to measure oxidizing triplet excited states in aerosol liquid water, Environ. Sci. Technol., In press, 2023.

Maizel, A. C. and Remucal, C. K.: The effect of probe choice and solution conditions on the apparent photoreactivity of dissolved organic matter., Environ. Sci. Process. Impacts, 19(8), 1040–1050, doi:10.1039/c7em00235a, 2017.

Manfrin, A., Nizkorodov, S. A., Malecha, K. T., Getzinger, G. J., McNeill, K. and Borduas-Dedekind, N.: Reactive oxygen species production from secondary organic aerosols: the importance of singlet oxygen, Environ. Sci. Technol., 53(15), 8553–8562, doi:10.1021/acs.est.9b01609, 2019.

McCabe, A. J. and Arnold, W. A.: Reactivity of triplet excited states of dissolved natural organic matter in stormflow from mixed-use watersheds., Environ. Sci. Technol., 51(17), 9718–9728, doi:10.1021/acs.est.7b01914, 2017.

McNeill, K. and Canonica, S.: Triplet state dissolved organic matter in aquatic photochemistry: reaction mechanisms, substrate scope, and photophysical properties., Environ. Sci. Process. Impacts, 18(11), 1381–1399, doi:10.1039/c6em00408c, 2016.

McNeill, V. F.: Aqueous organic chemistry in the atmosphere: sources and chemical processing of organic aerosols., Environ. Sci. Technol., 49(3), 1237–1244, doi:10.1021/es5043707, 2015.

Mekic, M., Brigante, M., Vione, D. and Gligorovski, S.: Exploring the ionic strength effects on the photochemical degradation of pyruvic acid in atmospheric deliquescent aerosol particles, Atmos. Environ., 185, 237–242, doi:10.1016/j.atmosenv.2018.05.016, 2018.

Monge, M. E., Rosenørn, T., Favez, O., Müller, M., Adler, G., Abo Riziq, A., Rudich, Y., Herrmann, H., George, C. and D'Anna, B.: Alternative pathway for atmospheric particles growth., Proc. Natl. Acad. Sci. USA, 109(18), 6840–6844, doi:10.1073/pnas.1120593109, 2012.

Ossola, R., Clerc, B. and McNeill, K.: Mechanistic insights into dissolved organic sulfur photomineralization through the study of cysteine sulfinic acid, Environ. Sci. Technol., 54(20), 13066–13076, doi:10.1021/acs.est.0c04340, 2020.

Parworth, C. L., Young, D. E., Kim, H., Zhang, X., Cappa, C. D., Collier, S. and Zhang, Q.: Wintertime water-soluble aerosol composition and particle water content in Fresno, California, J. Geophys. Res. Atmos., 122(5), 3155–3170, doi:10.1002/2016JD026173, 2017.

https://doi.org/10.5194/egusphere-2023-566
Preprint. Discussion started: 28 March 2023

Paulson, S. E., Gallimore, P. J., Kuang, X. M., Chen, J. R., Kalberer, M. and Gonzalez, D. H.: A light-driven burst of hydroxyl radicals dominates oxidation chemistry in newly activated cloud droplets., Sci. Adv., 5(5), eaav7689, doi:10.1126/sciadv.aav7689, 2019.

Reid, J. S., Koppmann, R., Eck, T. F. and Eleuterio, D. P.: A review of biomass burning emissions part II: intensive physical properties of biomass burning particles, Atmos. Chem. Phys., 5(3), 799–825, doi:10.5194/acp-5-799-2005, 2005.

Renard, P., Reed Harris, A. E., Rapf, R. J., Ravier, S., Demelas, C., Coulomb, B., Quivet, E., Vaida, V. and Monod, A.: Aqueous phase oligomerization of methyl vinyl ketone by atmospheric radical reactions, J. Phys. Chem. C, 118(50), 29421–29430, doi:10.1021/jp5065598, 2014.

Rossignol, S., Aregahegn, K. Z., Tinel, L., Fine, L., Nozière, B. and George, C.: Glyoxal induced atmospheric photosensitized chemistry leading to organic aerosol growth., Environ. Sci. Technol., 48(6), 3218–3227, doi:10.1021/es405581g, 2014.

Schauer, J. J., Kleeman, M. J., Cass, G. R. and Simoneit, B. R.: Measurement of emissions from air pollution sources. 3. C1-C29 organic compounds from fireplace combustion of wood., Environ. Sci. Technol., 35(9), 1716–1728, doi:10.1021/es001331e, 2001.

Smith, J. D., Sio, V., Yu, L., Zhang, Q. and Anastasio, C.: Secondary organic aerosol production from aqueous reactions of atmospheric phenols with an organic triplet excited state., Environ. Sci. Technol., 48(2), 1049–1057, doi:10.1021/es4045715, 2014.

Tan, Y., Lim, Y. B., Altieri, K. E., Seitzinger, S. P. and Turpin, B. J.: Mechanisms leading to oligomers and SOA through aqueous photooxidation: insights from OH radical oxidation of acetic acid and methylglyoxal, Atmos. Chem. Phys., 12(2), 801–813, doi:10.5194/acp-12-801-2012, 2012.

Tilgner, A., Bräuer, P., Wolke, R. and Herrmann, H.: Modelling multiphase chemistry in deliquescent aerosols and clouds using CAPRAM3.0i, J Atmos Chem, 70(3), 221–256, doi:10.1007/s10874-013-9267-4, 2013.

Tilgner, A. and Herrmann, H.: Tropospheric aqueous-phase OH oxidation chemistry: current understanding, uptake of highly oxidized organics and its effects, in Multiphase environmental chemistry in the atmosphere, vol. 1299, edited by S. W. Hunt, A. Laskin, and S. A. Nizkorodov, pp. 49–85, American Chemical Society, Washington, DC., 2018.

Tilgner, A., Schaefer, T., Alexander, B., Barth, M., Collett Jr., J. L., Fahey, K. M., Nenes, A., Pye, H. O. T., Herrmann, H. and McNeill, V. F.: Acidity and the multiphase chemistry of atmospheric aqueous particles and clouds, Atmos. Chem. Phys., 21(17), 13483–13536, doi:10.5194/acp-21-13483-2021, 2021.

https://doi.org/10.5194/egusphere-2023-566
Preprint. Discussion started: 28 March 2023

Urban, R. C., Lima-Souza, M., Caetano-Silva, L., Queiroz, M. E. C., Nogueira, R. F. P., Allen, A. G., Cardoso, A. A., Held, G. and Campos, M. L. A. M.: Use of levoglucosan, potassium, and water-soluble organic carbon to characterize the origins of biomass-burning aerosols, Atmos. Environ., 61, 562–569, doi:10.1016/j.atmosenv.2012.07.082, 2012.

Vidrio, E., Phuah, C. H., Dillner, A. M. and Anastasio, C.: Generation of Hydroxyl Radicals from Ambient Fine Particles in a Surrogate Lung Fluid Solution, Environ. Sci. Technol., 43(3), 922–927, doi:10.1021/es801653u, 2009.

Volkamer, R., San Martini, F., Molina, L. T., Salcedo, D., Jimenez, J. L. and Molina, M. J.: A missing sink for gas-phase glyoxal in Mexico City: Formation of secondary organic aerosol, Geophys. Res. Lett., 34(19), doi:10.1029/2007GL030752, 2007.

Wander, R., Neta, P. and Dorfman, L. M.: Pulse radiolysis studies. XII. Kinetics and spectra of the cyclohexadienyl radicals in aqueous benzoic acid solution, J. Phys. Chem., 72(8), 2946–2949, doi:10.1021/j100854a044, 1968.

Wang, X., Gemayel, R., Hayeck, N., Perrier, S., Charbonnel, N., Xu, C., Chen, H., Zhu, C., Zhang, L., Wang, L., Nizkorodov, S. A., Wang, X., Wang, Z., Wang, T., Mellouki, A., Riva, M., Chen, J. and George, C.: Atmospheric photosensitization: A new pathway for sulfate formation., Environ. Sci. Technol., 54(6), 3114–3120, doi:10.1021/acs.est.9b06347, 2020.

Washenfelder, R. A., Young, C. J., Brown, S. S., Angevine, W. M., Atlas, E. L., Blake, D. R., Bon, D. M., Cubison, M. J., de Gouw, J. A., Dusanter, S., Flynn, J., Gilman, J. B., Graus, M., Griffith, S., Grossberg, N., Hayes, P. L., Jimenez, J. L., Kuster, W. C., Lefer, B. L., Pollack, I. B., Ryerson, T. B., Stark, H., Stevens, P. S. and Trainer, M. K.: The glyoxal budget and its contribution to organic aerosol for Los Angeles, California, during CalNex 2010, J. Geophys. Res., 116(D21), doi:10.1029/2011JD016314, 2011.

Wenk, J., Aeschbacher, M., Sander, M., von Gunten, U. and Canonica, S.: Photosensitizing and inhibitory effects of ozonated dissolved organic matter on triplet-induced contaminant transformation, Environ. Sci. Technol., 49(14), 8541–8549, doi:10.1021/acs.est.5b02221, 2015.

Wenk, J. and Canonica, S.: Phenolic antioxidants inhibit the triplet-induced transformation of anilines and sulfonamide antibiotics in aqueous solution, Environ. Sci. Technol., 46(10), 5455–5462, doi:10.1021/es300485u, 2012.

Wenk, J., Eustis, S. N., McNeill, K. and Canonica, S.: Quenching of excited triplet states by dissolved natural organic matter., Environ. Sci. Technol., 47(22), 12802–12810, doi:10.1021/es402668h, 2013.

https://doi.org/10.5194/egusphere-2023-566
Preprint. Discussion started: 28 March 2023

Wenk, J., von Gunten, U. and Canonica, S.: Effect of dissolved organic matter on the transformation of contaminants induced by excited triplet states and the hydroxyl radical., Environ. Sci. Technol., 45(4), 1334–1340, doi:10.1021/es102212t, 2011.

Wilkinson, F., Helman, W. P. and Ross, A. B.: Rate constants for the decay and reactions of the lowest electronically excited singlet state of molecular oxygen in solution. an expanded and revised compilation, J. Phys. Chem. Ref. Data, 24(2), 663–677, doi:10.1063/1.555965, 1995.

Wong, J. P. S., Tsagkaraki, M., Tsiodra, I., Mihalopoulos, N., Violaki, K., Kanakidou, M., Sciare, J., Nenes, A. and Weber, R. J.: Atmospheric evolution of molecular-weight-separated brown carbon from biomass burning, Atmos. Chem. Phys., 19(11), 7319–7334, doi:10.5194/acp-19-7319-2019, 2019.

Wu, Z., Wang, Y., Tan, T., Zhu, Y., Li, M., Shang, D., Wang, H., Lu, K., Guo, S., Zeng, L. and Zhang, Y.: Aerosol liquid water driven by anthropogenic inorganic salts: implying its key role in haze formation over the North China Plain, Environ. Sci. Technol. Lett., 5(3), 160–166, doi:10.1021/acs.estlett.8b00021, 2018.

Xia, S.-S., Eugene, A. J. and Guzman, M. I.: Cross photoreaction of glyoxylic and pyruvic acids in model aqueous aerosol., J. Phys. Chem. A, 122(31), 6457–6466, doi:10.1021/acs.jpca.8b05724, 2018.

Zepp, R. G., Faust, B. C. and Hoigne, J.: Hydroxyl radical formation in aqueous reactions (pH 3-8) of iron(II) with hydrogen peroxide: the photo-Fenton reaction, Environ. Sci. Technol., 26(2), 313–319, doi:10.1021/es00026a011, 1992.

Zhang, H., Surratt, J. D., Lin, Y. H., Bapat, J. and Kamens, R. M.: Effect of relative humidity on SOA formation from isoprene/NO photooxidation: enhancement of 2-methylglyceric acid and its corresponding oligoesters under dry conditions, Atmos. Chem. Phys., 11(13), 6411–6424, doi:10.5194/acp-11-6411-2011, 2011.

Zhou, W., Mekic, M., Liu, J., Loisel, G., Jin, B., Vione, D. and Gligorovski, S.: Ionic strength effects on the photochemical degradation of acetosyringone in atmospheric deliquescent aerosol particles, Atmos. Environ., 198, 83–88, doi:10.1016/j.atmosenv.2018.10.047, 2019.

Zhou, X., Davis, A. J., Kieber, D. J., Keene, W. C., Maben, J. R., Maring, H., Dahl, E. E., Izaguirre, M. A., Sander, R. and Smoydzyn, L.: Photochemical production of hydroxyl radical and hydroperoxides in water extracts of nascent marine aerosols produced by bursting bubbles from Sargasso seawater, Geophys. Res. Lett., 35(20), doi:10.1029/2008GL035418, 2008.